1/26/9/14/79

DR. 055

GA-A15216
UC-77

MASTER

FORT ST. VRAIN MEU PROGRAM FINAL REPORT

Prepared under
Contract DE-AT03-76ET35300
for the San Francisco Operations Office
Department of Energy

DATE PUBLISHED: JULY 1979

DISTRIBUTED

GENERAL ATOMIC COMPANY

Printed in the United States of America
Available from
National Technical Information Service
U.S. Department of Commerce
5285 Port Royal Road
Springfield, Virginia 22161
Price: Printed Copy $5.25; Microfiche $3.00

DISCLAIMER

GA-A15216
UC-77

FORT ST. VRAIN MEU PROGRAM FINAL REPORT

Prepared under
Contract DE-AT03-76ET35300
for the San Francisco Operations Office
Department of Energy

GENERAL ATOMIC PROJECT 6400

DATE PUBLISHED: JULY 1979

GENERAL ATOMIC COMPANY

ABSTRACT

This report documents the status of a program to insert a nonproliferation MEU/Th fuel cycle into Fort St. Vrain. This program was discontinued in September 1978 when General Atomic, Gas Cooled Reactor Associates, and Public Service Company of Colorado all agreed to terminate the program in order to fully support necessary front-end licensing and design activities on HTGR-SC commercialization. The conclusions reached from core design and fuel cycle management studies are presented in detail. The report also presents the results of studies to provide a verified computer library of programs for use in design and analysis of MEU fuel for Fort St. Vrain; preliminary fuel performance models for the prediction of MEU fuel failure and safety evaluations; interim design data for Ag and Pu transport in MEU/Th fuel materials; and results of R/B studies on various MEU fuel kernels.

CONTENTS

FIGURES

TABLES

TABLES (Continued)

SUMMARY AND CONCLUSIONS

A detailed study was performed of a 20% enriched uranium fuel cycle for the FSV core. Included in this study was a transition from the present high enriched uranium (HEU) cycle to an all-MEU cycle on a segment-by-segment reload basis.

The conclusions reached from the fuel management and core design studies are:

1. The MEU cycle with 20% enrichment can operate satisfactorily with a 6-year lifetime after equilibrium is reached.

2. During the approach to equilibrium, region power peaking is excessive with 20% enrichment. A solution would be to step down the enrichment from 93% to 20% over several years; lumped burnable poison zoning could also provide a solution.

3. A one-step change to 20% enrichment could be acceptable if the fuel lifetime were reduced to 4 years.

4. The ratio of Th/U in fuel loaded would be about 2:1 for a 4-year cycle, but about 0.2:1 for a 6-year cycle.

5. A MEU cycle may have merit over a LEU cycle because of the flexibility in zoning with the thorium and the possibility for a demonstration of U-233 recycle.

6. Fuel cycle costs appear to be 10% to 50% higher for MEU than for HEU, assuming that the unit fabrication costs are equal.

7. Parametric fuel cycle calculations varying C/Th and the U-238 resonance integral failed to reveal but a small potential for reducing the resonance integral.

These conclusions illustrate that while an acceptable core design can be produced, the flexibility afforded to the designers is somewhat less than originally considered possible.

The development of a formally controlled library of verified computer programs for use in the design and analysis of MEU fuel in the FSV reactor was initiated. The essential elements of the system were:

1. Definition and permanent storage of base versions of the programs.

2. Use of data elements to store all changes to the program base versions in a sequential manner and permanent storage of these data elements.

3. Establishment of a central document file with information on each program and every update.

To meet tighter process and product specifications required for monitoring the quality of MEU fuel for FSV, several improved QC techniques are needed. In particular, methods are needed to establish levels of fuel failure during irradiation and MEU particle product quality. Four tasks were pursued:

1. Evaluation of particle fractionation by a liquid fluidized bed technique.

2. Calculational method for buffer void volume analysis.

3. SiC coating strength and flow measurement.

4. Residual chlorine measurement in TRISO coated particles.

Tighter process and product specifications required to maintain the quality of MEU fuel for FSV reloads need improved QC monitoring techniques. Four tasks were pursued to improve the current QC methodology:

1. Particle separation by a liquid fluidized bed technique to remove defective particles.

2. An improved calculational technique for buffer void volume analysis.

3. A technique for SiC coating strength and flow measurement.

4. Residual chlorine measurement on TRISO coated particles.

Particle fractionation was considered not to be cost effective and process improvements to improve product quality were suggested. In addition, the sphericity of the particles needs improvement. Studies have shown that SiC coating failure probably cannot be attributed to high residual chloride content of some particles. A better definition of this problem is recommended before additional QC method development work is undertaken.

Preliminary fuel performance models were developed for the prediction of MEU fuel failure in HTGR core design and safety evaluations. Models are included for TRISO MEU UC_2 and TRISO ThO_2 fuel. The phenomena treated are: (1) contamination, (2) missing or defective coatings, (3) kernel migration, (4) SiC - fission product reactions, and (5) failure at temperatures exceeding 1600° to 1800°C.

Available data for silver and plutonium transport in HTGR systems have been reviewed. The results were used as the basis for deriving interim design data for silver and plutonium transport in candidate MEU/Th fuel materials.

Measurements were completed of the R/B values for Kr-85m at 1100°C from various MEU (19.5% enrichment) fuel kernels and laser-failed MEU TRISO particles which were prepared for irradiation testing in FSV test elements FTE-2, -4, and -6 and in capsules HRB-14 and HRB-15B (ORNL high flux isotope reactor).

The difference in the R/B values of the various MEU kernels studied does not appear to be significant. For the laser-failed TRISO particle studies, the R/B values increase in the order of oxide kernels < oxycarbide kernels < carbide kernels. This difference appears to be due to the higher susceptibility to hydrolysis of the UC_2 phase, which may have occurred to a certain extent after laser-failing and prior to R/B measurements.

1. CORE DESIGN

1.1. SUMMARY

A detailed study was performed of a fuel cycle in the FSV core using 20% enriched uranium, the so-called MEU cycle. Included in this study was a transition from the present high enriched, or HEU cycle, to an all-MEU cycle on a segment-by-segment reload basis (Ref. 1-1).

This work was an extension of earlier feasibility studies on the use of nonproliferation fuel cycles in the HTGR (Refs. 1-2 through 1-4). These studies showed that transition cycles within FSV operating constraints were feasible for MEU fuel (20% enrichment) in 3-year semiannual and 4-year annual cycles, and for 6-year annual fuel cycles at 28% enrichment. Since the 6-year annual fuel cycle is now used for FSV operation, the present work was an attempt at a more detailed investigation of this cycle, using MEU fuel at 20% enrichment, to more precisely define the problems and potential solutions.

Results from this study basically confirm the earlier feasibility work; i.e., for a 6-year cycle at 20% enrichment, maximum region peaking factors exceeded current values at early time points during the first few transition cycles. However, the full equilibrium MEU core has a satisfactory power distribution. Based on the work performed, it is felt that the transition cycle problems can be alleviated by additional lumped burnable poison zoning, or additional axial fuel zoning and a change in thorium loading. Alternatively, the transition to MEU fuel can most easily be accomplished by reducing the enrichment to the 20% level in steps over a 2- or 3-year period. The FSV MEU program has been terminated and no further work is planned at this time.

1.2. NUCLEAR METHODS

As part of the FSV MEU program, a preliminary check of nuclear methods for MEU and LEU fuel was performed. The purpose of this check was to ensure that no major errors existed in the cross sections and codes for fuel calculations of this type. This preliminary study consisted of a series of check calculations with the GA reference cross-section generating code MICROX (Ref. 1-5) against a set of British WIMS-D code* results (which in turn have been compared with British LEU experimental results).

MICROX (Ref. 1-5) code calculations using HTGR reference data sets were compared to WIMS-D (Refs. 1-6, 1-7) calculations for some typical 20% enriched UO_2-graphite HTGR unit cells. The cases chosen for the comparison study are summarized in Table 1-1. The unit cell was chosen to be representative of that used for HTGR cross-section calculations and consisted of a fuel rod containing fuel particles surrounded by graphite moderator. The fuel rod diameter and the fuel kernel or grain diameter were varied as shown in Table 1-1 to cover a variety of cases.

A comparison of WIMS-D and MICROX results is shown in Table 1-2. (The WIMS-D calculations were performed by C. F. Griggs at Winfrith, England.) All of the cases assume a zero buckling and an isolated two-region unit cell. As can be seen from these results, the MICROX calculations agree quite well with the WIMS-D values, ranging from 0.7% to 1.8% larger in k_∞ values than the WIMS-D numbers.

Additional neutronic data comparisons are shown in Tables 1-3 and 1-4. These include two group (fast and thermal) constants and U-238 microscopic capture cross sections.

As indicated in Table 1-2, the use of ENDF/B-4 resonance data instead of the usual HTGR resonance data (based on ENDF/B-2 for U-238) yielded 0.2

---

*WIMS-D is a recent version of the WIMS code described in Refs. 1-6 and 1-7.

TABLE 1-1
CASE DEFINITIONS

Case	Description	Fuel Rod Radius (cm)	Cell Radius (cm)	Atom Density (atoms/barn-cm)					Temp. (K)
				Region 1				Region 2	
				C	O	U-235	U-238	C	
1	Reference HTGR	0.5	1.353	0.05	0.001	0.0001	0.0004	0.06	1100
2	Same as Case 1 except 800-μm grains	0.5	1.353	0.05	0.001	0.0001	0.0004	0.06	1100
3	Same as Case 1 except larger fuel rod radius	0.635	1.353	0.05	0.001	0.0001	0.0004	0.06	1100
4	Same as Case 1 except doubled UO_2 density	0.5	1.353	0.05	0.002	0.0002	0.0008	0.06	1100
5	Same as Case 1 except 300 K	0.5	1.353	0.05	0.001	0.0001	0.0004	0.06	300

TABLE 1-2
MICROX VERSUS WIMS-D k_∞ COMPARISONS

Case	Description	k_∞			
		WIMS-D	MICROX[a]	MICROX[b] Version 4 Resonance Data	MICROX[c] σ^{238} + 1.0 barn
1	Reference (1100 K)	1.56734	1.57859 (+0.7%)	1.57503 (+0.5%)	1.56520 (-0.1%)
2	800-μm grains (9 g/cm^3)	1.70612	1.67358 (-1.9%	1.67135 (-2.0%	1.65954 (-2.7%)
	800-μm grains (11 g/cm^3)		1.68816 (-1.1%)		1.67403 (-1.9%)
3	Increased fuel rod diameter	1.42747	1.45383 (+1.8%)	1.44925 (+1.5%)	1.43434 (+0.5%)
4	Doubled UO_2 density	1.43016	1.44599 (+1.1%)	1.44161 (+0.8%	1.42283 (-0.5%)
5	300 K	1.64104	1.65535 (+0.9%)	1.65173 (+0.7%)	1.64128 (0.0%)
	Temperature defect (1100-300 K)	-0.0737	-0.0768 (+4.2%)	-0.0767 (+4.1%)	-0.0761 (+3.2%)

[a] MICROX results with currently used ENDF/B Version 3 resonance integral data.

[b] MICROX results with new ENDF/B Version 4 resonance integrals.

[c] Case 1, but with an arbitrarily chosen correction to the U-238 basic resonance cross-section data used in MICROX.

TABLE 1-3
TWO GROUP CONSTANTS COMPARISON

		D		Absorption		$\nu\Sigma_f$		Flux	
		WIMS-D	MICROX	WIMS-D	MICROX	WIMS-D	MICROX	WIMS-D	MICROX
Case 1									
	Fast	1.644	1.607 (0.977)	8.190×10^{-4}	7.984×10^{-4} (0.975)	4.224×10^{-4}	4.223×10^{-4} (1.000)	327.6	326.6 (0.997)
	Thermal	1.229	1.225 (0.997)	3.343×10^{-3}	3.378×10^{-3} (1.010)	6.529×10^{-3}	6.583×10^{-3} (1.008)	218.9	218.8 (1.000)
Case 2									
	Fast	1.641	1.605 (0.978)	5.958×10^{-4}	6.417×10^{-4} (1.077)	4.178×10^{-4}	4.181×10^{-4} (1.001)	330.9	328.8 (0.994)
	Thermal	1.229	1.226 (0.997)	3.343×10^{-3}	3.281×10^{-3} (0.982)	6.529×10^{-3}	6.388×10^{-3} (0.978)	240.1	240.4 (1.001)
Case 3									
	Fast	1.667	1.630 (0.978)	1.178×10^{-3}	1.138×10^{-3} (0.966)	6.511×10^{-4}	6.560×10^{-4} (1.007)	323.6	322.7 (0.997)
	Thermal	1.240	1.236 (0.997)	4.845×10^{-3}	4.906×10^{-3} (1.013)	9.528×10^{-3}	9.633×10^{-3} (1.001)	127.7	128.9 (1.010)
Case 4									
	Fast	1.641	1.606 (0.978)	1.267×10^{-3}	1.246×10^{-3} (0.984)	7.893×10^{-4}	7.980×10^{-4} (1.011)	316.1	315.0 (0.997)
	Thermal	1.218	1.214 (0.997)	5.668×10^{-3}	5.734×10^{-3} (1.012)	1.116×10^{-2}	1.128×10^{-2} (1.011)	105.8	105.9 (1.001)
Case 5									
	Fast	1.643	1.606 (0.978)	7.312×10^{-4}	7.057×10^{-4} (0.965)	4.260×10^{-4}	4.236×10^{-4} (0.994)	328.9	327.8 (0.997)
	Thermal	1.217	1.193 (0.980)	4.513×10^{-3}	4.558×10^{-3} (1.010)	4.558×10^{-3}	8.992×10^{-3} (1.008)	168.3	168.6 (1.002)

TABLE 1-4
U-238 MICROSCOPIC CAPTURE CROSS SECTIONS AND FRACTIONAL CAPTURES

		σ_c^{238}		U-238 Fractional Capture	
		WIMS-D	MICROX	WIMS-D	MICROX
Case 1					
	Fast	9.895	9.490(-0.41B) (0.959)	0.1771	0.1693 (0.956)
	Thermal	1.090	1.102 (1.011)	0.01304	0.01317 (1.010)
Case 2					
	Fast	5.879	6.680(+0.80B) (1.136)	0.1063	0.1200 (1.129)
	Thermal	1.090	1.070 (0.982)	0.01430	0.01406 (0.983)
Case 3					
	Fast	8.561	8.043(-0.52B) (0.939)	0.2441	0.2287 (0.937)
	Thermal	1.014	1.027	0.01141	0.01167 (1.023)
Case 4					
	Fast	6.915	6.649(-0.27B) (0.962)	0.2388	0.2288 (0.958)
	Thermal	0.9725	0.9843	0.01124	0.01139 (1.013)
Case 5					
	Fast	8.241	7.774(-0.47B) (0.943)	0.1481	0.1392 (0.940)
	Thermal	1.423	1.436 (1.009)	0.01308	0.01323 (1.012)

to 0.3% lower calculated eigenvalues. The HTGR cross-section sets will be updated to include these revised data. Such a change was not important for HEU systems since the U-238 contribution is negligible there. The MICROX and WIMS-D results can also be brought into good agreement if 1 barn is added to the U-238 capture cross section above 2.38 eV (excluding Case 2) (see Table 1-2). However, while providing some insight into the nature of cross-section discrepancies, this sort of arbitrary change is not based on detailed experimental data (such as ENDF/B-4) and cannot be extrapolated with confidence. Cases 3 and 4 are somewhat puzzling in that MICROX and WIMS-D appear to respond slightly differently to an increase in fuel rod diameter as opposed to an increase in UO_2 density at the same fuel rod diameter. The differences may be due to the use of the same input Bell factor in WIMS-D when the fuel rod diameter or density was changed (see subsequent discussion).

The results for Case 2 in which 800-μm-diameter grains were assumed are also somewhat puzzling. The computed eigenvalues are not precisely comparable because of the neglect of thermal region grain shielding in the WIMS-D calculation. A UO_2 density of 8.966 g/cm^3 in 800-μm grains was assumed for the results given in Table 1-2 through 1-4 (grain volume fraction of 0.025). If the UO_2 density is raised to the theoretical maximum of 10.97 g/cm^3 (grain volume fraction of 0.02043), the U-238 fast capture cross section computed by MICROX is reduced by about 6%. This change is not nearly enough to resolve the 18% to 20% U-238 fast capture cross-section discrepancy shown for Case 2 in Table 1-4 (Cases 1, 3, 4, and 5 are 4% to 6% low, whereas Case 2 is 14% high).

The grain shielding treatment in the WIMS-D code depends upon the calculation of an input Bell (or Levine) factor (Ref. 1-8) which accounts for both grain and rod shielding according to some analytic procedure (see Ref. 1-9 for a description of one such procedure). The Bell factor used in the WIMS-D cases without grains was 1.16, whereas the WIMS-D Case 2 used an input Bell factor of 0.013. The Bell factor should, in principle,

vary with the cell geometry and atom densities, which fact may account for some of the differences between MICROX and WIMS-D for Cases 3 and 4.

The MICROX code uses a grain shielding treatment developed by Wälti (Ref. 1-9). According to Stamatelatos (Ref. 1-10), Wälti's method should tend, if anything, to overestimate the grain shielding, i.e., produce too small a cross section. With the MICROX code producing substantially larger resonance cross sections than the WIMS-D code for Case 2, no simple explanation for the discrepancy is apparent.

The agreement in computed temperature coefficients is very good. This result, along with the good agreement in the values, would indicate that there are no serious errors in the calculational methods for HTGR physics design with MEU fuel.

1.3. REFERENCES

1-1. Fehrenbach, M. E., and A. Baxter, "Core Design Calculations for MEU Fuel in FSV," General Atomic Report, to be published.

1-2. Asmussen, K. E., and J. T. Ganley, "Core Design and Feasibility Study for LEU- and MEU/Th-Fueled HTGRs," DOE Report GA-A14757, General Atomic Company, June 1978.

1-3. Merrill, M. H., and R. K. Lane, "Medium-Enriched Uranium/Thorium Fuel Cycle Parametric Studies for the HTGR," DOE Report GA-A14659, General Atomic Company, December 1977.

1-4. Asmussen, K. E., et al., "Low-Enrichment and Denatured (Thorium) Fuels for the HTGR: A Status Report," General Atomic Report GA-A14606, September 1977.

1-5. Merrill, M. H., "Nuclear Design Methods and Experimental Data in Use at Gulf General Atomic," Gulf General Atomic Report Gulf-GA-A12652 (GA-LTR-2), July 1973.

1-6. Askew, J. R., et al., "A General Description of the Lattice Code WIMS," J. Brit. Nucl. Energy Soc. 5, 564 (1966).

1-7. Roth, M. J., et al., "The Preparation of Input Data for WIMS," United Kingdom Atomic Energy Authority Report AEEW-R 538, 1967.

1-8. Levine, M. M., "Resonance Integral Calculations for U-238 Lattices," Nucl. Sci. Eng. 16, 271 (1963).

1-9. Wälti, P., "Evaluation of Grain Shielding Factors for Coated Fuel Particles," Nucl. Sci. Eng. 45, 321 (1971).

1-10. Stamatelatos, M. G., "Rational Approximations for Cross-Section Space-Shielding in Doubly Heterogeneous Systems," Nucl. Sci. Eng. 61, 543 (1976).

2. FUEL CYCLE MANAGEMENT

2.1. ALTERNATIVE FUEL ELEMENT DESIGN STUDIES

Parametric fuel cycle calculations were carried out in which the C/Th ratio and the U-238 resonance integral were treated as independent variables. This work is reported in Refs. 2-1 and 2-2 and is therefore only summarized here. In the initial calculations the physics characteristics were not fixed to a specific design of the fuel element. Subsequently, a set of 14 different fuel block designs was examined; these designs had previously been evaluated from a thermal performance standpoint for the HEU cycle in either FSV or the LHTGR. The objective was to determine if any of these designs, which featured different numbers and sizes of fuel and coolant holes, might have U-238 resonance integrals substantially below those of the reference fuel block designs. A small computer program was written to evaluate the resonance integrals based on correlations with fuel element geometry developed in previous MEU cycle work. To date, the designs evaluated show only a small potential for reductions in the resonance integral. This is not too surprising since these designs were originally selected as part of a survey of thermal hydraulic performance. Further evaluations with this code are planned for elements which are more specifically oriented toward low resonance integrals.

2.2. REFERENCES

2-1. "HTGR Generic Technology Program: Materials Technology, Reactor Operating Experience, Medium-Enriched-Uranium Fuel Development, Quarterly Progress Report for the Period Ending April 30, 1978," DOE Report GA-A14962, General Atomic Company, May 1978.

2-2. "HTGR Generic Technology Program: Fuels and Core Development, Quarterly Progress Report for the Period Ending August 31, 1978," DOE Report GA-A15093, General Atomic Company, September 1978.

3. FUEL DEVELOPMENT

3.1. SUMMARY

Preliminary fuel performance models are provided for the prediction of MEU fuel failure in HTGR core design and safety evaluations. Models are included for TRISO MEU UC_2 and TRISO ThO_2 fuel. The phenomena treated are: (1) contamination, (2) missing or defective coatings, (3) kernel migration, (4) SiC - fission product reactions, and (5) failure at temperatures exceeding 1600° to 1800°C. Pressure vessel models are not included since evaluation of this phenomenon is continuing.

Available data for silver and plutonium transport in HTGR systems have been reviewed. The results were used as the basis for deriving interim design data for silver and plutonium transport in candidate MEU/Th fuel materials.

3.2. FUEL PERFORMANCE MODELS AND PARTICLE DESIGNS

Preliminary MEU fuel performance models are presented. The phenomena treated for TRISO MEU UC_2 and TRISO ThO_2 models are: (1) contamination, (2) missing or defective coatings, (3) kernel migration, (4) SiC - fission product reactions, and (5) failure at temperatures exceeding 1600° to 1800°C.

HTGR fuel performance is a function of particle design, fast neutron exposure, kernel burnup, and irradiation temperature. Coating designs are based upon the peak fast neutron exposure and kernel burnup expected for a given particle type. To provide the maximum amount of flexibility, the performance models are given as a function of the fraction of peak fast neutron exposure and kernel burnup for which any coating is designed.

3.2.1. TRISO MEU UC_2 Models

Contamination. The fuel specification is written to assure an expected value for heavy metal contamination less than 1×10^{-4} and/or an R/B for Kr-85m of 3×10^{-5} at 1100°C (Ref. 3-1). The specification states with 95% confidence that the R/B for Kr-85m will be less than 4×10^{-5} at 1100°C. The expected value for the R/B for Kr-85m will therefore be assumed to be 3×10^{-5} at 1100°C; it will be assumed with 95% confidence that the R/B for Kr-85m will be less than 4×10^{-5} at 1100°C.

A lower confidence bound for release due to heavy metal contamination was arrived at assuming that only bare kernels make up a heavy metal contamination fraction of 1.0×10^{-4}. The R/B for Kr-85m for bare 200-μm UO_2 kernels in a fuel rod is 4×10^{-2} at 1100°C (Ref. 3-2). Assuming (1) that the R/B for bare 200-μm UC_2 kernels in a fuel rod is 4×10^{-2} and (2) that the R/B varies as the inverse of kernel diameter, the R/B for Kr-85m from bare MEU UC_2 kernels (350-μm diameter) in a fuel rod would be 2.3×10^{-2}. The lower limit for Kr-85m release due to contamination is therefore 2.3×10^{-6} at 1100°C. The Kr-85m release fraction due to contamination will be estimated using

$$R/B_{cont,1100°C} = C_x \ (3 \times 10^{-5}) \quad , \tag{3-1}$$

where C_x is the correlation parameter at confidence level x. Values for C_x are $C_5 = 0.08$, $C_{50} = 1.0$, and $C_{95} = 1.33$.

Fuel with Missing or Defective Coatings. The failure fraction due to the presence of fuel manufactured with missing or defective coatings (f_d) is estimated from

$$f_d = C_{f,x} \left(\frac{BU}{BU_{max}}\right) \left(C_{p,x}\right) 0.002 \quad , \tag{3-2}$$

where $C_{f,x}$ = probability, at confidence level x, that a particle will fail,

$\left(C_{p,x}\right)0.002$ = value, at confidence level x, for the fraction of fuel having missing or defective coatings,

BU/BU_{max} = ratio of kernel burnup (% FIMA) to the maximum burnup (% FIMA) expected in a reactor core.

Values for $C_{f,x}$ and $C_{p,x}$ are given in Table 3-1.

TABLE 3-1
CORRELATION PARAMETERS NEEDED TO ESTIMATE FAILURE FRACTIONS DUE TO PRESENCE OF FUEL MANUFACTURED WITH MISSING OR DEFECTIVE COATINGS

Correlation Parameter	Confidence Level		
	5%	50%	95%
$C_{f,x}$	0.50	0.70	1.00
$C_{p,x}$	0.38	0.75	1.5

The product of $C_{p,95}$ and 0.002 is 0.003, which is consistent with the HTGR fuel product specification for the maximum allowable fraction of TRISO particles having missing or defective coatings. The expected value [$C_{p,x}$ = 0.75, 0.75(0.002) = 0.0015] is one-half of the maximum population allowed by the specification.

Pressure Vessel Behavior. Pressure vessel performance for TRISO MEU fissile fuel is being evaluated. When completed, models will be provided at 5%, 50%, and 95% confidence levels.

Kernel Migration. Failure due to kernel migration will be assumed if a migrating kernel contacts the SiC layer of a TRISO MEU particle. The best estimate of the kernel migration coefficient (KMC_{50}) for UC_2 kernels is (Ref. 3-3)

$$KMC_{50}\ (m^2\text{-}K/s) = 0.62 \exp\left(\frac{-3.113 \times 10^5}{8.313T}\right) . \qquad (3\text{-}3)$$

Values for KMC at a 5% or 95% confidence level are estimated from

$$KMC_x = C_x \, KMC_{50} \quad , \tag{3-4}$$

where $C_5 = 0.351$ and $C_{95} = 2.850$. The predicted failure fraction equals the probability that a migrating kernel contacts the SiC layer. The distribution of distances between UC_2 kernels and the SiC layer is described by an average of $(\bar{t}_B + 35)$ μm, where $\bar{t}_B$ is the average buffer thickness, and a standard deviation (σ_t) of

$$\sigma_t \ (\mu m) = \left\{(0.174\bar{t}_B)^2 + [0.163(35)]^2\right\}^{1/2} \quad . \tag{3-5}$$

The average inner PyC thickness (35 μm) and fractional standard deviations in the buffer (0.174) and inner PyC (0.163) thicknesses are those values assumed when developing TRISO MEU fuel designs. The average buffer thickness ($\bar{t}_B$) can only be determined after the peak expected kernel burnup and fast neutron exposures are known.

SiC - Fission Product Reactions. The thickness of the SiC on TRISO UC_2 fuels is decreased during irradiation due to reactions with lanthanide fission products and palladium. The failure fraction associated with this phenomenon is set equal to the probability that the SiC thickness on any particle is reduced by 50%. The expected distribution of SiC thicknesses is described by an average value of 35 μm and a standard deviation of 5.0 μm. Failure by this mechanism is assumed to cause metallic fission product release but no gaseous release.

The rates of SiC - fission product reactions are shown as a function of temperature in Fig. 3-1. Two regimes are indicated. Data above ∿1400°C were collected from postirradiation thermal gradient heating of HEU TRISO UC_2 (Ref. 3-4). The best estimate for the rate of change in SiC thickness ($\dot{X}_{50}$) in this regime is

$$\dot{X}_{50} \ (\mu m/h) = 4.2 \times 10^7 \exp\left(\frac{-3.283 \times 10^5}{8.313T}\right) \quad , \tag{3-6}$$

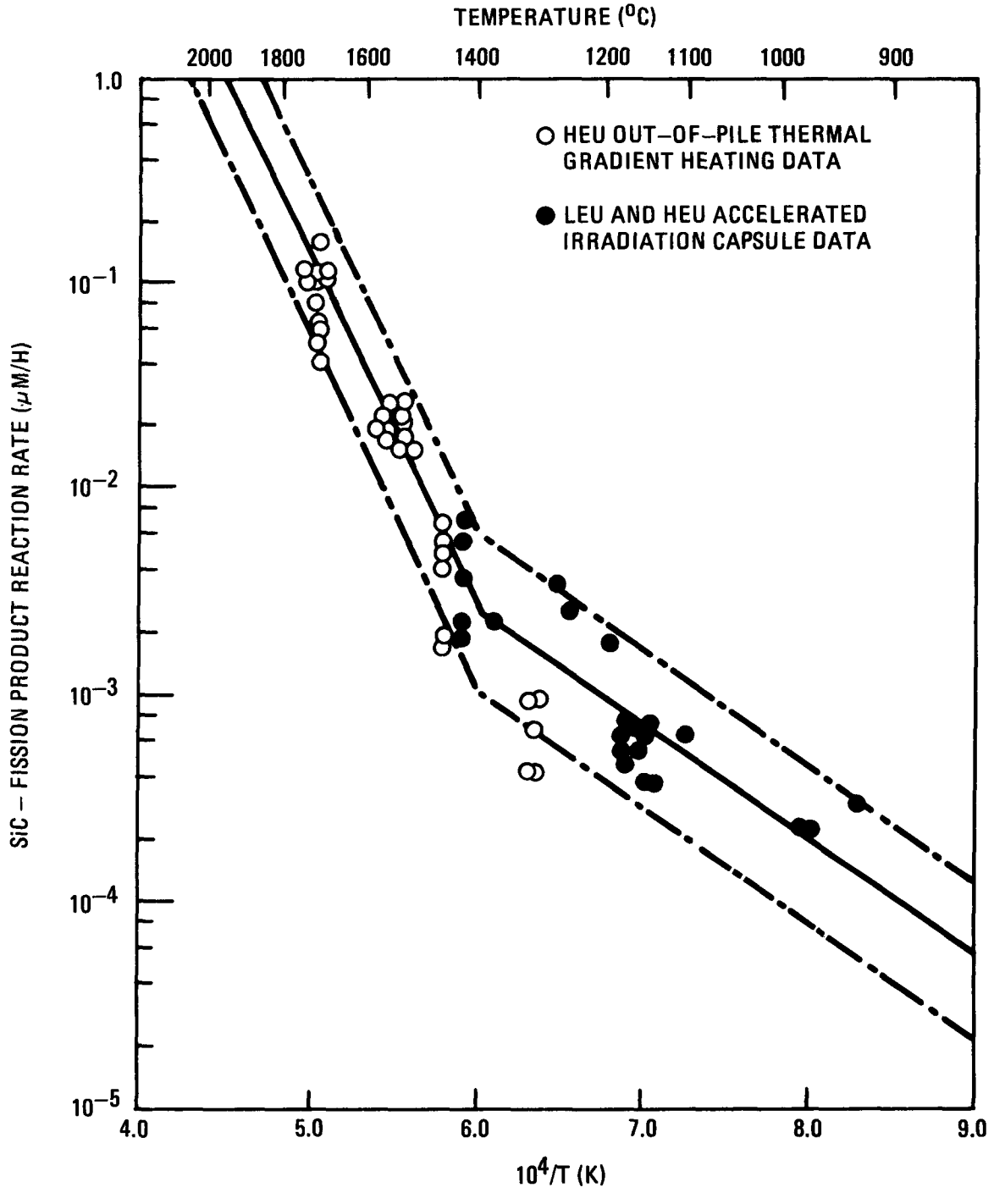

Fig. 3-1. Variation in SiC - fission product reaction rate with inverse temperature assumed for TRISO MEU UC_2

where T is temperature (K). The rate at a 5% or 95% confidence level is defined by

$$\dot{X}_x \ (\mu m/h) = C_x \dot{X}_{50} \quad , \tag{3-7}$$

where $C_5 = 0.46$ and $C_{95} = 2.18$.

Data for the lower temperature regime (T less than about 1400°C) were collected from observations of Pd-SiC attack in HEU and LEU fuels during PIE of accelerated irradiation capsules (Refs. 3-5 through 3-8). The change in SiC thickness with time in this regime is

$$\dot{X}_{50} \ (\mu m/h) = 6.43 \exp\left(\frac{-1.08 \times 10^5}{8.313T}\right) \quad . \tag{3-8}$$

Correlation parameters for this regime are $C_5 = 0.45$ and $C_{95} = 2.23$. The kinetics expression yielding the maximum rate of attack should be used for any condition. For example, assuming best estimates for reaction rates, Eq. 3-6 should be used at $T \geq 1416°C$, while Eq. 3-8 should be used for $T < 1416°C$.

The reactions described by Eqs. 3-6 and 3-8 will not begin until an adequate supply of fission products is generated. To be consistent with HEU models, it is assumed that the reaction rates are zero for MEU UC_2 kernel burnups $\leq$1.0% FIMA.

Failure at Temperatures Exceeding 1600° to 1800°C. Temperatures exceeding 1600° to 1800°C are generally only expected during the hypothetical accidents that are evaluated for reactor licensing and siting arguments. These conditions generally lead to a reactor scram and a loss of forced circulation followed by a rise in fuel temperature due to decay heat. There is no thermal gradient under these conditions; consequently, the rates of SiC - fission product reactions and kernel migration approach

zero. The model provided in this section is empirical in nature and accounts for the following coating failure mechanisms: (1) pressure vessel; (2) thermal degradation of the IPyC, SiC, and OPyC layers; (3) coating - fission product reactions under isothermal conditions; and (4) actinide metal dispersion.

Failure fractions at temperatures above 1600° to 1800°C are assumed for HEU UC_2 to increase linearly from the predicted pressure vessel value at 1600° to 1800°C to 1.0 at 2000°C (Ref. 3-3). The critical temperature (T_{crit}) at which the transition occurs is defined as a function of HEU kernel burnup. The HEU TRISO UC_2 models had no provision for estimating the uncertainty in predicted fraction at temperatures exceeding T_{crit}. Models for TRISO MEU fuel will be provided at 5%, 50%, and 95% confidence levels as an indication of the uncertainty associated with fuel failure during hypothetical accidents.

The 95% confidence level model is essentially identical to that for HEU UC_2. Failure fractions are assumed to increase linearly from the 95% confidence value for the pressure vessel failure fraction at T_{crit} to 1.0 at 2000°C, where

$$T_{crit}\ (°C) = 1800 \tag{3-9}$$

for $BU/BU_{max} \leq 20/78 = 0.256$ or

$$T_{crit}\ (°C) = -269(BU/BU_{max}) + 1869 \tag{3-10}$$

for $BU/BU_{max} > 0.256$. These values for T_{crit} are identical to those for HEU TRISO UC_2 at any given ratio of BU/BU_{max}. This mechanism will be assumed to operate on the unfailed fuel in a core each time T_{crit} is exceeded and, in the event of extended times above T_{crit}, each 100 hours.

Models at 5% and 50% confidence levels are based on core heatup simulation tests (CHSTs) of TRISO HEU ThC_2, $(Th/U)C_2$, and UC_2 fuels (Ref. 3-9)

Four tests have been run. The data indicate that a single failure model may be possible for TRISO dicarbide fuels, that is, at very high temperatures, independent of actinide metal composition and kernel burnup. This was assumed when developing the models.

The 50% confidence model was defined from the variation in average failure fraction with temperature for the four TRISO dicarbide CHSTs. The model assumes (1) a linear increase in failure fraction from the expected value for the pressure vessel failure fraction at T_{crit} (Eq. 3-10) to 0.039 at 2050°C and (2) a linear increase in failure fraction (independent of irradiation exposure) from 0.039 at 2050°C to 1.0 at 2450°C.

The 5% confidence model was based on the best behavior observed in a TRISO dicarbide CHST (HEU UC_2 test 78 IHR-B-5-1). This model assumes (1) a linear increase in failure fraction from the 5% confidence value for the pressure vessel failure fraction at T_{crit} (Eq. 3-10) to 0.025 at 2200°C, and (2) a linear increase in failure fraction (independent of irradiation exposure) from 0.025 at 2200°C to 1.0 at 2500°C.

The data used to develop the 5% and 50% confidence models were collected from CHSTs in which temperatures were increased from ∿1100° to ∿2500°C in time periods ranging from 8 to 80 hours. Assuming an 80-hour test, the time t (hours) that test samples experienced temperatures exceeding T_i(°C) is

$$t = 142.9 - 0.057T_i \quad . \tag{3-11}$$

If, in any core design evaluation utilizing the 5% or 50% confidence models, fuel experiences temperatures above T_{crit} for times longer than indicated by Eq. 3-11, the resulting failure fraction will be assumed to increase to values predicted by the 95% confidence limit model.

3.2.2. TRISO ThO_2 Models

Heavy Metal Contamination. The approach used to define Kr-85m R/B from ThO_2 contamination is the same as that shown for MEU UC_2. Values for C_{95} and C_{50} are the same as those for MEU UC_2. The value for C_5 is 0.06 to account for the larger diameter of the ThO_2 kernels (450 μm).

Fuel With Missing or Defective Coatings. The model and input parameters provided for TRISO MEU UC_2 fuel are used in conjunction with ThO_2 values for BU_{max}.

Pressure Vessel Behavior. Pressure vessel performance for TRISO ThO_2 fertile fuel is being evaluated. When completed, models will be provided at 5%, 50%, and 95% confidence levels.

Kernel Migration. The fraction of fuel that fails because of kernel migration will be assumed equal to the probability that a migrating kernel contacts the SiC layer of TRISO ThO_2. The distribution of distances between kernels and SiC layers is defined by an average value of $(\bar{t}_B + 35)$ μm, where $\bar{t}_B$ is the average buffer thickness, and a standard deviation of $\{(0.174\bar{t}_B)^2 + [0.163(35)]^2\}^{1/2}$.

Kernel migration distances will be estimated with the model now used for BISO coated ThO_2 kernels (Ref. 3-3). Migration distances are estimated using the ThO_2 KMC. Two periods must be considered when predicting ThO_2 kernel migration. During the incubation period (θ), no migration occurs (KMC = 0). The KMC will be assumed 0 (1) if kernel burnups are less than 2% FIMA, and (2) if $\sum_i (t_i/\theta_i) < 1$, where t_i is the time (s) at temperature T_i.

The best estimate for θ_i is

$$\theta_{i_{50}}\ (s) = 4.7 \times 10^{-4} \exp\left(\frac{-3.16 \times 10^5}{8.313T}\right) \quad , \tag{3-12}$$

where T is temperature (K). Values for θ_i at various confidence levels are estimated using

$$\theta i_x \text{ (s)} = C_x \theta i_{50} \quad , \tag{3-13}$$

where $C_5 = 0.32$ and $C_{95} = 3.12$. The quantity $\Sigma\ t_i/\theta_i$ will be evaluated beginning with the start of irradiation in any local region. If either criterion 1 or 2 is exceeded, ThO_2 kernel migration distance is estimated using the ThO_2 KMC which is given by

$$KMC_{50}\ (m^2 \cdot K/s) = 0.39 \exp\left(\frac{-2.96 \times 10^5}{8.313T}\right) \quad . \tag{3-14}$$

The uncertainty in KMC is estimated from

$$KMC_x = C_x\ KMC_{50} \quad , \tag{3-15}$$

where $C_5 = 0.24$ and $C_{95} = 4.22$.

SiC - Fission Product Reactions. No SiC - fission product reactions are expected in TRISO ThO_2 fuel.

Failure At Temperatures Above 1600° to 1800°C. Models are provided at 5%, 50%, and 95% confidence levels. The 95% confidence model is identical to that given for TRISO MEU UC_2 except that the value for BU_{max} used in Eqs. 3-9 and 3-10 will be for ThO_2 rather than UC_2.

The 5% and 50% confidence models are based on TRISO ThO_2 CHST results (Ref. 3-10). The model at 50% confidence assumes (1) a linear increase in failure fraction from the expected pressure vessel failure fraction at T_{crit} (Eqs. 3-9 and 3-10) to 0.023 at 2100°C, and (2) a linear increase in failure fraction (independent of irradiation exposure) from 0.023 at 2100°C to 1.0 at 2500°C. At 5% confidence, the model assumes that the failure fraction does not increase from the 5% confidence found for

pressure vessel failure at T_{crit} (Eqs. 3-9 and 3-10) until temperatures reach 2350°C. Failure fractions increase linearly with temperature from the value at 2350°C to 1.0 at 2500°C (independent of irradiation exposure). The time dependence for the 5% and 50% confidence limit TRISO ThO_2 models will be the same as given for TRISO MEU UC_2.

3.3. SILVER AND PLUTONIUM TRANSPORT STUDIES

In the development of MEU fuel for application in HTGR systems, the transport behavior of plutonium and silver is of particular interest because inventories of plutonium and silver isotopes are relatively high in MEU fuel compared with HEU fuel. Plutonium migrates at a higher rate than uranium and thorium, and the tolerable release of plutonium into an HTGR primary circuit is small, mainly because Pu-238 has such a high bone inhalation effectivity (rem/Ci, about 500 times that of Sr-90). Silver transport is an important consideration because Ag-110m is an important contributor to man-rem exposures in certain maintenance operations.

3.3.1. Silver Transport

Available data for silver transport relative to MEU fuel were reviewed in Ref. 3-11. The results of this review were used to develop interim design data for silver transport in candidate MEU/Th fuel material (Ref. 3-12). In developing these design data, it was assumed that (1) the candidate fissile MEU kernels are dense UC_2, UCO, and UO_2; (2) the reference fissile particle coating is TRISO; and (3) the reference fertile particle is BISO coated ThO_2. (Note: TRISO coated ThO_2 will constitute the licensing basis for FSV MEU reloads.)

In summary of the interim design data, the assumption of no appreciable holdup of silver in carbide and oxycarbide kernels is recommended. An equation is recommended for use in calculating reduced diffusion coefficients for the release of silver from oxide kernels. No appreciable holdup of

silver in BISO coatings is recommended. For TRISO coated particles, recommendations are (1) no appreciable release of silver below 1200°C, and (2) release by a diffusion process above 1200°C.

3.3.2. Plutonium Transport

Available information on plutonium transport in HTGR systems was reviewed in Ref. 3-11. Results of this review were used as the basis for deriving interim design data for plutonium transport in candidate MEU/Th fuel material (Ref. 3-12). In deriving these design data, it was assumed that (1) the candidate fissile MEU fuel kernels are dense UC_2, UCO, and UO_2; (2) the reference fissile particle coating is TRISO; and (3) the reference fertile particle is BISO coated ThO_2. (Note: TRISO coated ThO_2 will constitute the licensing basis for FSV MEU reloads.)

In summary of the interim design data, an equation is recommended for use in calculating reduced diffusion coefficients for the release of plutonium from carbide and oxycarbide kernels. It is recommended that (1) the diffusion coefficient for plutonium in oxide kernels be assumed to be a factor of 10 lower than that in carbide kernels, (2) no appreciable holdup of plutonium in BISO coatings be assumed, and (3) no appreciable release of plutonium from intact TRISO coated particles be assumed.

An analysis was made by K. J. Mysels (GA) to estimate the amount of plutonium that could be released from the core into the primary circuit of a large HTGR. The analysis showed that the amount of plutonium that could evaporate through the graphite-helium boundary layer is about an order of magnitude less than the tolerable amount in the primary circuit of a large [3360-MW(t)] HTGR. The conclusion drawn from the calculation is that the effective vapor pressure of low concentrations of plutonium will be so much lower than that of pure Pu_2C_3 that the release will be negligible even if the transport of plutonium through graphite is in no way limiting. Details of this analysis are presented in Ref. 3-13.

3.4. REFERENCES

3-1. "Technical Support Document for Issue C of the HTGR Fuel Product Specification," General Atomic Report GA-A14450, to be published.

3-2. Myers, B. F., et al., "The Behavior of Fission Product Gases in HTGR Fuel Material," DOE Report GA-A13723, General Atomic Company, October 1977.

3-3. "Fuel Design Data Manual, Issue C," General Atomic Report GA-A14429, to be issued.

3-4. Smith, C. L., "SiC - Fission Product Reactions in TRISO UC_2 and WAR UC_xO_y Fissile Fuel, Part I: Kinetics of Reactions in a Thermal Gradient," General Atomic Report GA-A14313, September 1977.

3-5. Young, C. A., and C. B. Scott, "Postirradiation Examination of Capsule P13Q," ERDA Report GA-A14174, General Atomic Company, September 1977.

3-6. Homan, F., et al., "Irradiation Performance of HTGR Fuel Rods in HFIR Experiments HRB-4 and 5," ERDA Report ORNL-5115, Oak Ridge National Laboratory, June 1976.

3-7. Tiegs, T., Oak Ridge National Laboratory, personal communication regarding capsule HT-33.

3-8. Kovacs, W. J., General Atomic Company, personal communication regarding capsule P13T.

3-9. General Atomic unpublished data.

3-10. General Atomic unpublished data.

3-11. "HTGR Fuels and Core Development Program, Quarterly Report for the Period Ending February 28, 1978" DOE Report GA-A14863, General Atomic Company, March 1978.

3-12. "HTGR Generic Technology Program: Materials Technology, Reactor Operating Experience, Medium-Enriched Uranium Fuel Development, Quarterly Report for the Period Ending April 30, 1978," DOE Report GA-A14962, General Atomic Company, May 1978.

3-13. "HTGR Generic Technology Program: Materials Technology, Reactor Operating Experience, Medium-Enriched Uranium Fuel Development, Quarterly Report for the Period Ending July 31, 1978," DOE Report GA-A15066, General Atomic Company, August 1978.

4. METHODS

4.1. CONTROLLED COMPUTER PROGRAM LIBRARY

The major work item funded under this task was the initiation of the development of a formally controlled library of verified computer programs for use in the design and analysis of MEU fuel in the FSV reactor. This was planned to be an effort that would extend over 3 years and be completed in 1980.

After an initial review of the project, it was decided that the first step should be the implementation of a formal system to control any changes or extensions to the programs under consideration. Approximately 25 major programs were identified as requiring this control. A system was then identified that provided an appropriate balance between the conflicting requirements of formal control and the desire of the design groups to have program updates made rapidly. The essential elements of the system are:

1. Definition and permanent storage of base versions of the programs.

2. Use of data elements to store all changes to these base versions in a sequential manner and the permanent storage of these data elements.

3. Establishment of a central document file with information on each program and every update.

This system was implemented and appears to be functioning quite well.

With the system in place, the collection of existing data on past code verification efforts began, and the amount of additional work needed

to meet formal verification requirements was defined. It was intended that this verification effort would continue in FY-79; however, with the cancellation of the FSV MEU program, the schedule will need to be reevaluated to be consistent with the needs of the generic HTGR program.

4.2. U-238 DATA

A final work item under this task was the processing of the ENDF/B-5 nuclear data for U-238. This was not completed because the data were never issued by the national ENDF/B committee.

5. MEU FUELS QUALITY CONTROL (QC) TEST TECHNIQUE DEVELOPMENT

5.1. INTRODUCTION

The need to introduce MEU fuels (20% enriched) into FSV leads to more restrictive fuel product specifications. The tighter process and product specifications require the development of more sensitive QC methods for measuring critical product attributes related to MEU fuel irradiation stability.

The increased levels of plutonium generated from U-238 conversion in low enriched (20% enriched U-235) MEU fuel particles require that a smaller fraction of the fuel particle coatings experiences pressure vessel failure. Also, a reduction in the circulating fission product activity in the gas turbine high-temperature gas-cooled reactor (GT-HTGR) results in economical operation of the plant due to fewer and less expensive maintenance outages.

5.2. PROGRAM OBJECTIVES

In order to assure that MEU fuels meet the tighter product specifications required for the GT-HTGR fuel, the existing processes for preparing MEU fuels must be improved. Also, improved QC techniques for product attribute measurement are needed.

Several product attributes which can adversely affect the irradiation stability of MEU fuels have been identified during irradiation experiments

at GA and ORNL during the past few years. These attributes include the following:

1. Number of particles with thin, broken, or missing coatings in a batch (defective particles).

2. Particles with large kernels and insufficient buffer void volume to accommodate internal fission gas pressure.

3. Highly faceted particles or doublets with high stresses in the outer low-temperature isotropic (OLTI) and SiC layers.

4. SiC coatings with large void areas (gold spots) and weak rupture strengths.

5. TRISO coated fuel particles with high levels of residual chloride which can attack the SiC layers during irradiation causing premature failure.

Assessment of the adequacy of QC test techniques for measuring these key attributes of MEU fuels slated for introduction into FSV was conducted under this program. The QC test methods evaluated were as follows:

1. A liquid fluidized bed particle fractionation system was evaluated as a means of isolating highly defective particles from MEU fuels for the determination of defective particle fractions.

2. The buffer void volume fraction, after the deposition of inner low-temperature isotropic (ILTI) layers, was measured to determine the loss in void due to impregnation of the buffer layers by coating gas species.

3. The SiC coating rupture strength for coated fuel particles with lenticular flaws in the SiC coatings was measured to determine if a routine QC measurement technique could be developed.

4. QC techniques for measuring the residual chloride in TRISO coated MEU particles were evaluated.

5.3. SUMMARY OF PROGRAM ACCOMPLISHMENTS

5.3.1. Particle Fractionation Studies

The removal of highly defective particles from a coated fuel particle batch by a liquid fluidized particle bed apparatus was studied as a means of separating these materials from the particle batch for QC measurement. Also, this system was evaluated as a method for improving the overall batch quality by removing defective particles.

The liquid fractionation system was successful in semi-quantitatively removing highly defective particles with missing coatings, broken kernels with half coatings, highly faceted particles, large kernels with thin buffer/ILTI coating thicknesses, doublet coated kernels, and bare kernels. Unfortunately, defective particles with more subtle defects such as cracked coatings could not be isolated from the particle batch with the fractionation unit. Therefore, its usefulness as a quantitative QC method for measuring defective particles in a coated fuel particle batch was limited. It was recommended that this unit not be used as a quantitative method for isolating defective MEU particles for QC measurement of the fraction of defective particles.

The semi-quantitative removal of highly defective particles from the batch showed that it is possible to improve the overall coated particle batch quality by use of the fractionation system. Defective particles with missing coating layers, doublet coated fuel kernels, highly faceted

coated half kernels, high porosity OLTI layers, and low heavy metal densities were separated in the initial and final particle fractions elutriated from the particle bed column. However, the cost penalty for improving coated particle product quality by this method appeared to be excessive. In the case of a low quality ThC_2 coated particle batch fractionated in this study, approximately 20% of the batch had to be removed to separate the highly defective particles. This represented a 80% yield of product for the fractionation step in the process.

For the 350-μm ThO_2 TRISO coated particles made in the dry coater at small load sizes (3 kg of ThO_2 kernels), the as-made product quality was improved. Fractionation of this material showed that elutriation of "weak sister" particles was possible. As occurred with the previous low quality coated ThC_2, the doublet particles and large kernels with thin buffer coatings were removed in the last elutriation fraction.

As a QC technique for isolating defective particles for quantitative measurement of the defective particle fractions, the liquid fluidized bed fractionation unit proved to be inadequate. However, as a means for removing highly defective particles from a coated particle batch, the fractionation unit offers a potential method to improve overall product quality. Unfortunately, the utilization of this technique may not be practical from a cost/benefit ratio. Improvement in product quality through process development probably represents a more cost effective means to make MEU fuel for the GT-HTGR. It is nearly impossible to make coated fuel particles without some defective particles being present in the batch. Therefore, it is recommended that the liquid fluidized bed particle fractionation apparatus be retained as a means of cleaning the particle batches, which is required before the fuel rods are made. Removal of the few highly defective particles in this cleaning step would not represent a large cost penalty.

5.3.2. Buffer Void Volume QC Measurement Method

The fraction of buffer void volume remaining after deposition of the ILTI coating on MEU coated fuel particles was determined. The impregnation of the buffer by coating gas species during ILTI deposition results in less void volume being available to accommodate high gas pressure from fission products and carbon monoxide. A QC method to measure the actual buffer void volume after the deposition of ILTI layers was developed and demonstrated on MEU fuel particles for the FSV MEU program.

5.3.3. QC Method to Measure SiC Rupture Strengths and Flaws

The SiC layer is the main barrier to fission product release. Failure of this coating results in high release of cesium, strontium, and plutonium to the surrounding graphite and ultimately to the helium coolant circuit. SiC coatings with large void areas (gold spots) were expected to have lower rupture strengths. Therefore, an assessment of the SiC layers with large flaws was required. The purpose of this program was to determine if an inexpensive routine QC test to measure the strength and the flaws in the SiC layers could be developed. Other than the simple compression point load breakage tests, no simple QC method to measure SiC rupture stresses could be found by the Test Techniques Development Branch (TTDB). The compression breakage of the SiC layers under a load was expected to be different from the tensile rupture of SiC layers due to excess internal fission gas pressure.

An extensive test program to measure the tensile burst strength of SiC layers with void areas (gold spots) was conducted by the Fuel Materials Branch (FMB) in parallel with TTDB's work (Ref. 5-1). The FMB used a hydraulic burst test developed by the UKAEA at the Springfield Nuclear Laboratories in England. This test consisted of measurement of the hydraulic tensile rupture strength of half shells of separated SiC coatings.

The TTDB and the FMB studies showed that the strength of SiC layers was not adversely affected by the void areas. The compression rupture and the hydraulic tensile rupture of the SiC layers were both unaffected by the size of the void areas. The factor which was most detrimental to the SiC coating strength was the shape of the coated fuel particle. Highly faceted, nonspherical coated fuel particles showed lower SiC rupture strengths. Severe faceting due to elliptical deformation of the coating reduced both the compression and tensile rupture strengths of the SiC layers. Doublet coated fuel kernels exhibited the lowest SiC coating rupture strengths. For moderately faceted coated fuel particles with polyhedron coating deformation, the mean rupture strength of the SiC coatings was not affected, but the standard deviation (scatter) in the rupture strength was increased.

The conclusions of these studies were that the SiC coating rupture strength is not affected by flaws but is affected by the coated particle shape. For MEU coated fuel particles, sphericity of the particles should be maintained at some minimum level. The current proposed coated particle aspect ratio specification of $\leq$1.20 (particle maximum diameter divided by particle minimum diameter) should be applied to eliminate any severe problems with degradation of the SiC coating strength. No new QC method development is required on this basis if particle faceting is controlled. Elimination of doublet coated fuel particles is particularly important to assure good SiC coating integrity for MEU fuels.

5.3.4. Residual Chloride in TRISO Coated Particles

The presence of residual chloride in TRISO coated fuel particles after deposition of the SiC coatings has been attributed to premature failure of the SiC coatings during irradiation (Ref. 5-2). An investigation of several batches of irradiation control particle samples was conducted to determine if a routine QC method for measuring residual chloride in TRISO coated fuel particles could be developed.

A review of all possible QC techniques to quantitatively measure residual chloride in TRISO coated fuel particles was made (Ref. 5-3). Some of the techniques considered were activation analysis, X-ray fluorescence, mass spectroscopy, electron scanning, microprobe, and pyrohydrolysis with trace Cl^- electrode titration. The pyrohydrolysis technique was selected as the best method for this analysis, based on the extensive amount of work done with this technique during FSV core 1 and segment 7 manufacture (Ref. 5-4). Thirty-two blind samples were submitted from three high SiC coating failure batches and two low SiC coating failure batches (historical irradiation samples) for pyrohydrolysis and scanning electron microscopic analyses with the following results:

1. The pyrohydrolysis technique and the electron microscopic analyses of historical irradiation particle batches show that the levels of residual chloride in these UC_2 TRISO coated particle samples were in the range of $\leq$30 ppm.

2. No differences in residual chloride level were noted between samples with high and low SiC coating failure during irradiation.

The absence of chloride ($\leq$30 ppm) in samples with both high and low SiC coating failures indicated that residual chloride was not the cause of differences in the irradiation behavior of the two types of coated particles. However, it is possible that the pyrohydrolysis technique for measuring residual chloride was in error. Therefore, scanning electron microscope and X-ray emission probe analyses of the materials were conducted. No residual chloride was detected in these analyses, which confirmed that the levels of residual chloride were low.

On this basis, it appeared that SiC coating failure observed could not be attributed to high residual chloride content. The need for a QC test to measure residual chloride in TRISO coated particles on a routine QC basis for MEU fuels for FSV was questioned. Better definition of this

problem is needed before any additional work is warranted. Careful control of the connected porosity in the ILTI coatings is recommended as the best means to eliminate chloride retention during SiC coating deposition.

5.4. DISCUSSION OF EXPERIMENTAL RESULTS

5.4.1. Particle Fractionation Studies

Separation of "weak sister" particles from a particle batch by the liquid fluidized particle bed method (Fig. 5-1) is possible because of the presence of coated fuel particles with variations in diameter and density in a parent particle batch. The elutriation (terminal velocity μT) of a particle from a fluidized particle bed is based on its drag coefficient (C_d), Reynolds number (Re), particle diameter (D_p), fluid density (ρ_ℓ), particle density (ρ_s), and the fluid viscosity (μ) (Ref. 5-5). For spherical particles in the range of HTGR fuel particles with Reynolds numbers in the range of 0.4 to 500, the terminal velocity μT is defined by the following equation:

$$\mu T \text{ (spherical)} = \frac{4}{225}\left[\frac{(\rho_s - \rho_\ell)^2 \, g^2}{\mu \rho_s}\right]^{1/3} D_p \quad , \qquad (5\text{-}1)$$

where ρ_s = density of coated particle,

ρ_ℓ = density of fluid,

μ = viscosity of fluid,

D_p = diameter of particles,

g = gravity coefficient.

The potential for removal of highly defective particles ("weak sisters") from a particle batch was indicated during the design of the liquid fluidized bed particle washing system for FSV fuel particles (Ref. 5-5). Evaluations of this system with several types of TRISO coated particles were

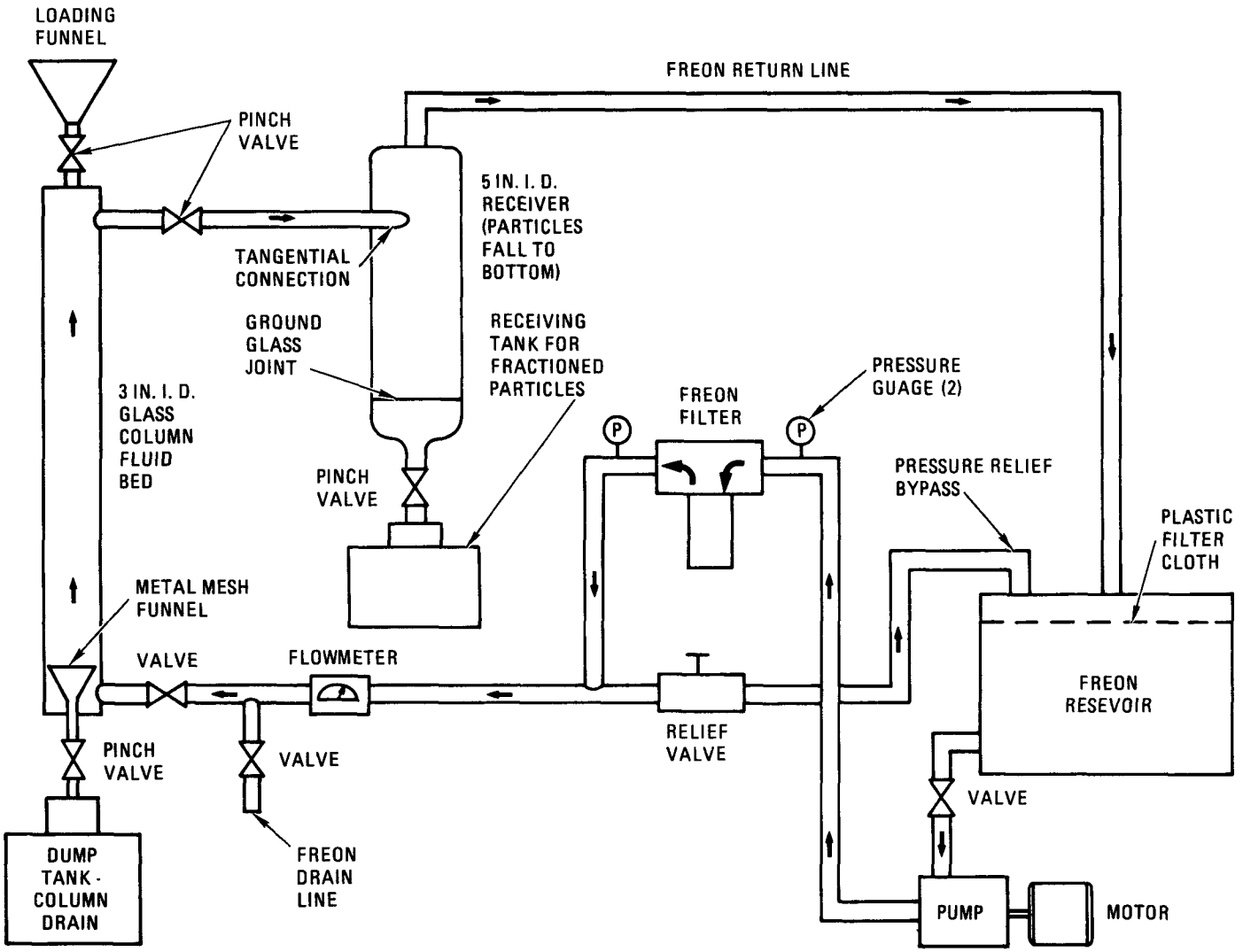

Fig. 5-1. Liquid fluidized particle bed fractionating system

conducted. The detailed results of the analyses were reported in Refs. 5-6 through 5-8. The major findings were as follows:

1. FSV Fertile B TRISO Coated Particles (Refs. 5-6, 5-7). The partial removal of "weak sister" particles with high faceting, large kernels with thin buffer/ILTI coatings, large SiC coating strength variations, large SiC coating flaws, low heavy metal densities, and high microporosity in the OLTI coatings was possible with low quality fertile B fuel particles. QC data for the nine aliquots fractionated are given in Table 5-1. Plots of these data (Figs. 5-2 through 5-5) are self-explanatory in that they show changes in the mean QC properties of the aliquots elutriated as a function of time. Most of the undesir- particles in the batch were contained in the first and last aliquots elutriated. Particle properties such as missing coatings, highly faceted coated particles, and high fraction of defective SiC coatings were found in these aliquots.

2. ThO_2 (350-μm) TRISO Coated Particles (Ref. 5-8). TRISO coated ThO_2 (350 μm) particles prepared during coating process development of MEU fuels were fractionated to determine if product quality could be improved by isolation of defective particles. The improvement in overall product quality was substantially less with this material than was observed with the FSV fertile B TRISO coated particles. These samples were prepared in the dry coater at very small batch sizes (3 kg of ThO_2 kernels). Therefore, the product quality of these materials was substantially better than the fertile material as fabricated. Data for these samples are given in Tables 5-2 and 5-3.

The buffer and ILTI layers could not be distinguished in the particle X-rays; therefore, the sum of the two is given. As can be seen in Tables 5-2 and 5-3, the overall particle size decreased in the later particle

TABLE 5-1
PROPERTIES OF FERTILE B ThC_2 TRISO COATED PARTICLES AFTER LIQUID FLUIDIZED BED FRACTIONATION
(BATCH 7344-33)

Aliquot No.	Weight (g)	Percent of Batch	Particle Diameter (μm)	Buffer + ILTI Thickness (μm)	SiC Thickness (μm)	OLTI Thickness (μm)	Hg Particle Density (g/cm^3)	Thorium (g Th/cm^3 of particles)	Total Particle Faceting, D_{max}/D_{min}	SiC Breakage Load, 50 Particles (kg)	OLTI Breakage Load, 50 Particles (kg)	Fraction of Defective SiC Coatings		SiC Flaws, Visual (% gold spots)	Missing Coatings			BAF OLTI	OLTI Sink Float Density (g/cm^3)
												Aliquot	Contribution to Batch		Buffer + ILTI	SiC	OLTI		
Original batch	4280	100	828 ± 54	107 ± 14	33 ± 2	36 ± 6	3.31	1.56	1.057 ± 0.037	NM[a]	NM	9.5×10^{-4}	1.00	~30	0/800	0/800	0/800	NM	1.95
2	10	0.2	699 ± 76	116 ± 17	34 ± 5	38 ± 8	2.15	0.52	1.128 ± 0.107	2.28 ± 0.502	1.71 ± 0.181	1.0×10^{-2}	2.0×10^{-5}	~50-60	0/900	5/900	0/900	1.048 ± 0.0083	1.94
3	30	0.7	685 ± 58	115 ± 16	30 ± 4	37 ± 7	2.59	0.92	1.088 ± 0.060	2.32 ± 0.441	1.77 ± 0.157	3.9×10^{-3}	2.7×10^{-5}	~30-40	0/1100	3/1100	2/1100	1.045 ± 0.0064	1.94
4	250	6.0	749 ± 69	105 ± 15	37 ± 4	37 ± 5	2.79	1.20	1.073 ± 0.049	2.28 ± 0.356	1.74 ± 0.159	3.0×10^{-3}	1.8×10^{-4}	~10	0/800	1/800	0/800	1.054 ± 0.0052	1.93
5	635	15.0	837 ± 70	113 ± 19	32 ± 3	38 ± 6	3.12	1.44	1.062 ± 0.035	2.29 ± 0.317	1.77 ± 0.115	7.7×10^{-4}	1.2×10^{-4}	~10	0/1000	0/1000	0/1000	NM	1.92
6	1050	25.0	842 ± 42	108 ± 13	29 ± 3	34 ± 6	3.29	1.59	1.043 ± 0.028	2.31 ± 0.257	1.75 ± 0.129	8.4×10^{-4}	2.1×10^{-4}	~10	0/900	0/900	0/900	NM	1.93
7	970	23.0	836 ± 46	105 ± 12	31 ± 3	36 ± 4	3.31	1.67	1.047 ± 0.032	2.26 ± 0.236	1.79 ± 0.129	6.0×10^{-4}	1.4×10^{-4}	~10	0/1000	0/1000	0/1000	1.049 ± 0.0051	1.92
8	450	11.0	836 ± 35	103 ± 12	31 ± 4	32 ± 5	3.38	1.77	1.050 ± 0.029	2.28 ± 0.258	1.71 ± 0.130	9.0×10^{-4}	9.9×10^{-5}	~10	0/1000	0/1000	0/1000	1.057 ± 0.0053	1.97
9	760	18.0	852 ± 71	96 ± 13	34 ± 3	31 ± 5	3.54	1.77	1.072 ± 0.100	2.28 ± 0.221	1.79 ± 0.118	7.0×10^{-4}	1.3×10^{-4}	~10	2/800	0/800	1/800	NM	1.93

(a) NM = not measured.

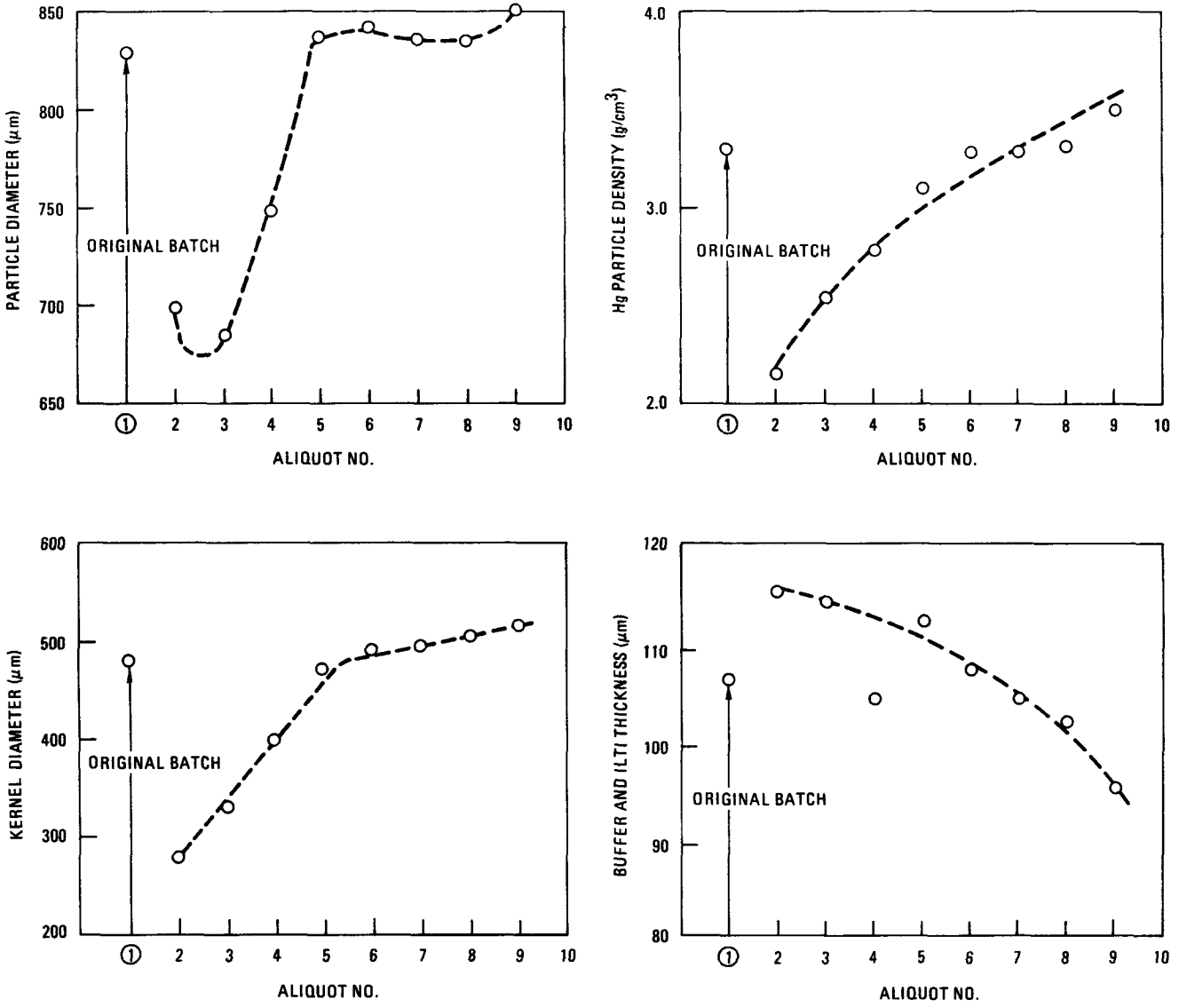

Fig. 5-2. Changes in particle diameter, kernel diameter, Hg particle density, and buffer + ILTI thickness

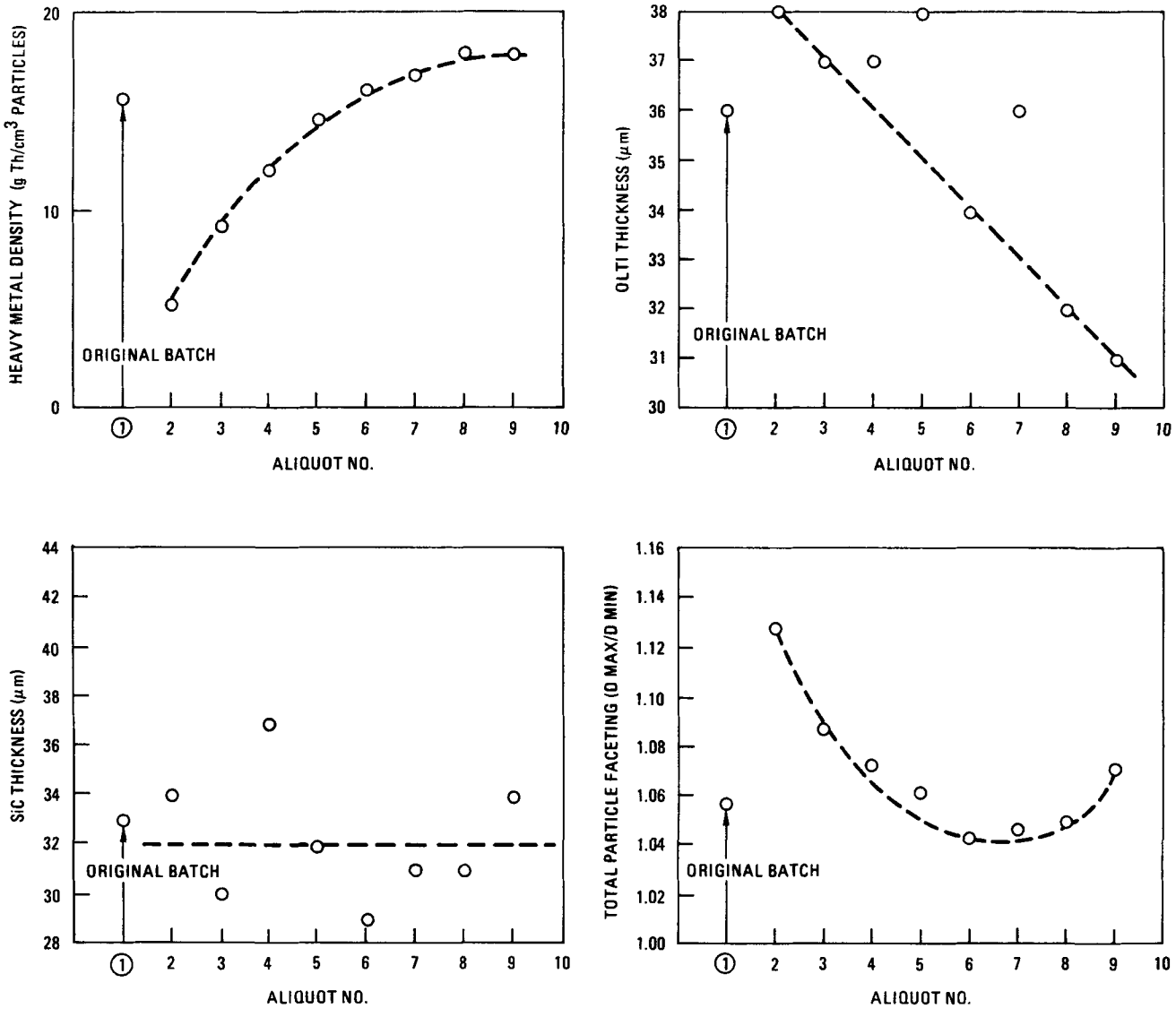

Fig. 5-3. Changes in heavy metal density, SiC thickness, OLTI thickness, and total particle faceting

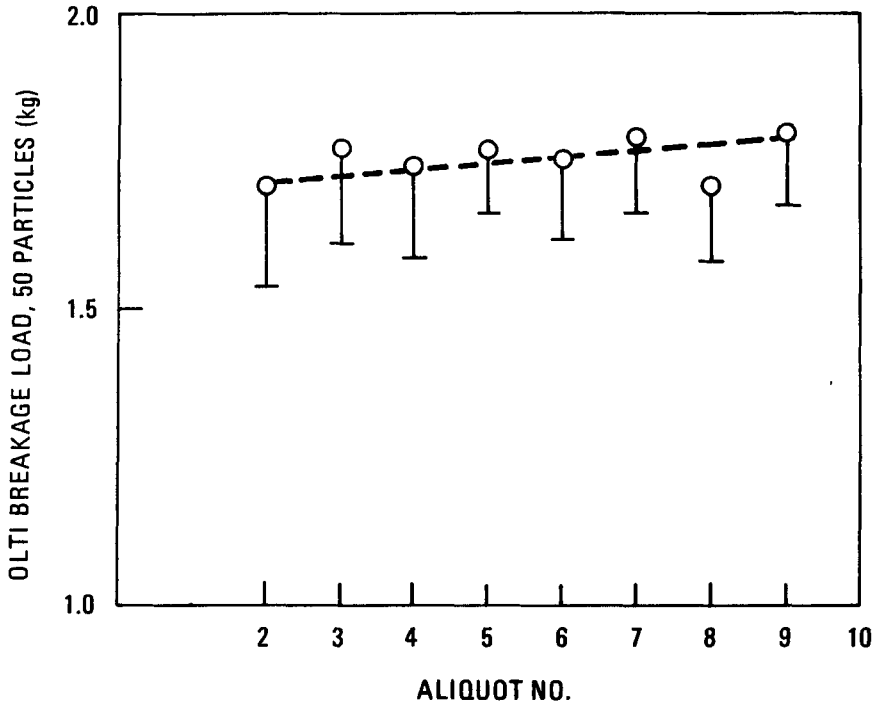

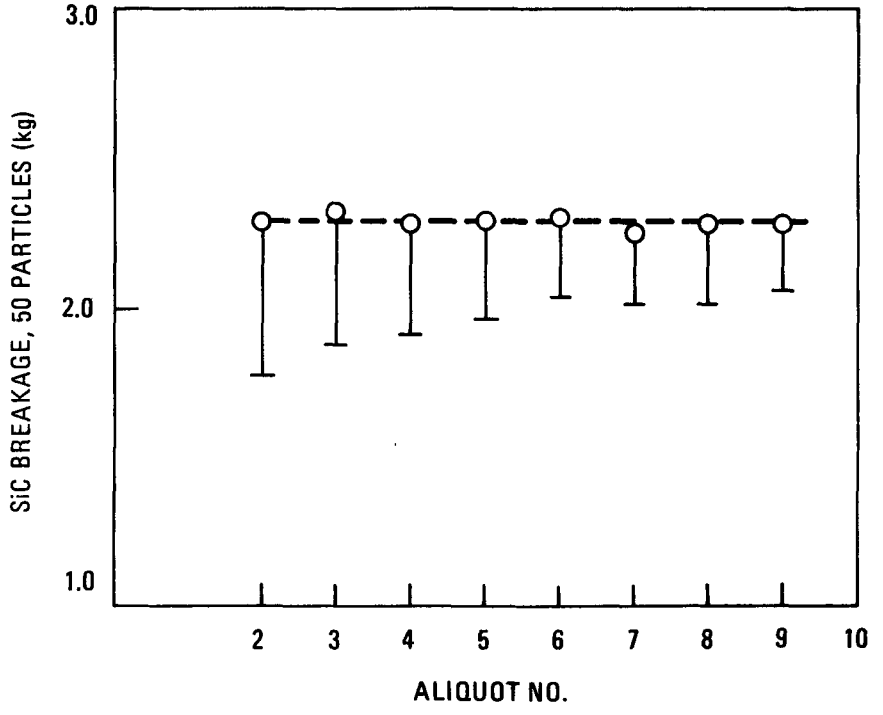

Fig. 5-4. Changes in OLTI breakage load and SiC breakage

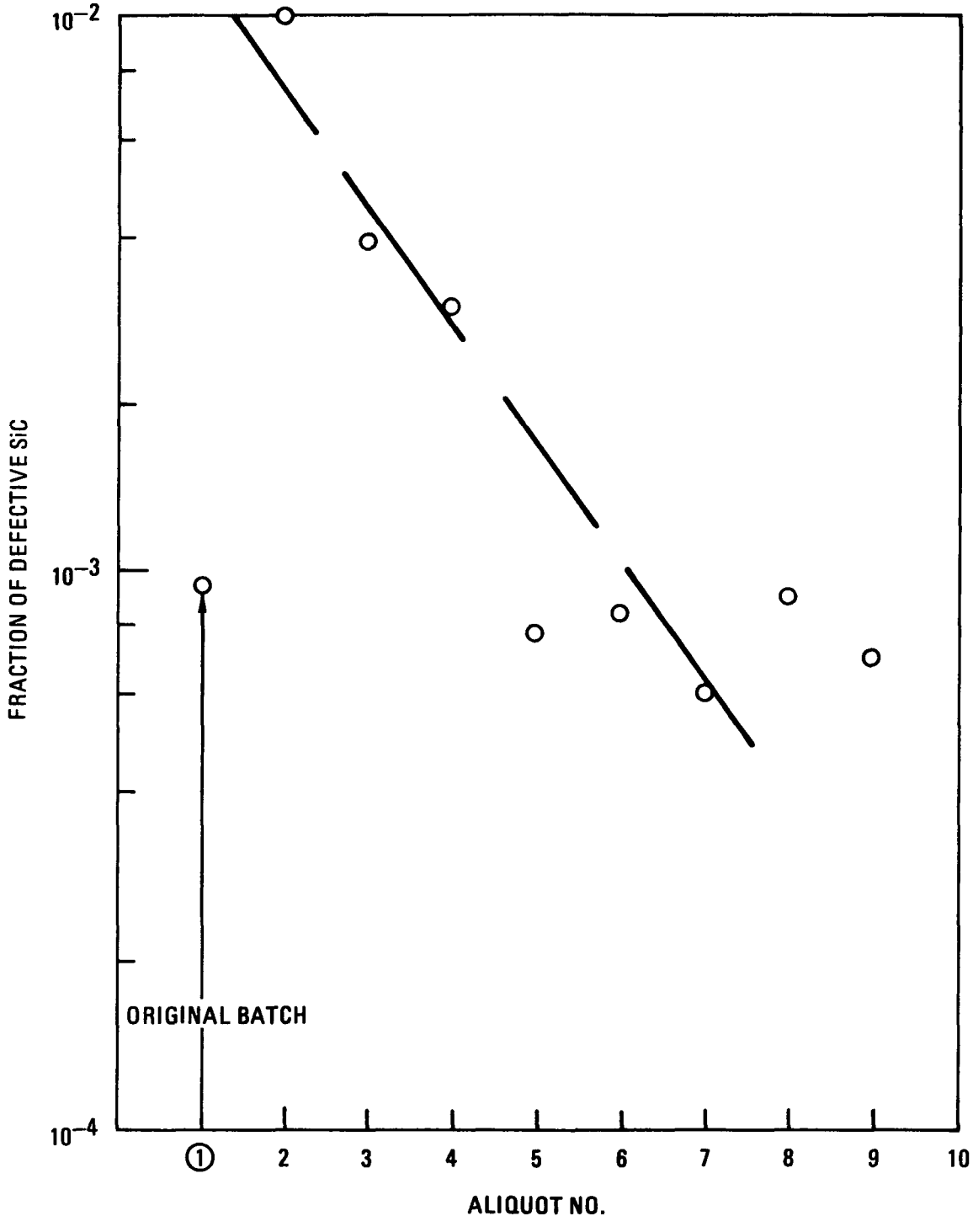

Fig. 5-5. Changes in fraction of defective SiC

TABLE 5-2
FRACTIONATION DATA FOR BATCH 6157-08-39T

Fraction	Particle Diameter (μm)	Kernel Diameter (μm)	Buffer + ILTI (μm)	SiC (μm)	OLTI (μm)
Original	772	357	142	34	41
39T-1	812	346	160	37	41
39T-2	786	354	146	35	40
39T-3	772	353	140	35	40
39T-4	759	354	131	34	40
39T-5	754	368	124	35	40

TABLE 5-3
FRACTIONATION DATA FOR BATCH 6157-08-40T

Fraction	Particle Diameter (μm)	Kernel Diameter (μm)	Buffer + ILTI (μm)	SiC (μm)	OLTI (μm)
Original	792	359	136	37	43
40T-1	824	348	156	37	44
40T-2	800	355	144	38	44
40T-3	783	356	141	34	44
40T-4	776	357	135	34	43
40T-5	766	364	127	35	44

fractions, as did the thickness of the combined buffer-ILTI layer. Kernel size increased slightly in the last fraction elutriated and decreased slightly in the first fraction elutriated. The SiC and OLTI layer thickness did not vary in the five fractions. No significant differences were found when the faceting, particle density, mercury intrusion, SiC crush strength, and OLTI crush strength were measured in the five elutriated fractions. The BAF_o values for the OLTI were also similar for these fractions.

A large number of doublet particles (0.4% in 6157-08-40T-5 and 1.0% in batch 6157-08-39T-5) were found in the last (No. 5) fraction. Doublet particles are not as strong as well-shaped single particles. Therefore, the fractionating process is worthwhile if it removes these particles, which are probably present in the original batch in a concentration of about 6×10^{-4}. [This fraction was determined by multiplying the doublet percentage found in the No. 5 fraction (-0.4% and 1.0%) by the percentage of fraction No. 5 present in the whole batch (16.8% and 6.0%, respectively).] The doublets are prime candidates for failure and fission gas release because they have highly stressed coatings and contain much more fissionable material than single particles.

The use of the liquid fractionation fluidized particle bed system for quantitatively isolating defective particles from a coated fuel particle batch was shown not to be practical as a QC measurement technique, and its application is not recommended. However, its utilization as a means for isolating those few highly defective particles from a batch appears feasible and is recommended. The cost penalties for removing all defective particles from the batch would result in low yields and high costs. Therefore, improvement in product quality through process development is probably a more economical method.

5.4.2. Buffer Void Volume Analysis

The primary purpose of a low density buffer layer is to accommodate internal fission gas and carbon monoxide pressure during irradiation of the fuel particle. The present GA fuel specifications define the necessary void volume by specifying the buffer density and thickness. The buffer density is measured prior to deposition of the ILTI coatings; therefore, the final buffer void volume is reduced by coating gas penetration and deposition in the buffer layers (Refs. 5-9, 5-10).

A calculational QC method for the measurement of buffer void volume after deposition of the ILTI coating was developed for MEU fuels. This QC method consists of solving the following equations:

1. Calculation of the combined ILTI carbon density (D_c) using Eq. 5-2:

$$D_c = \frac{W_c \, D_p \, D_k}{D_k - D_p \, (1 - W_c)} \quad , \tag{5-2}$$

where D_c = combined buffer-ILTI density,
D_p = particle density (at 250 psi),
D_k = kernel density (at 250 psi),
W_c = weight fraction of carbon (in particles).

2. Calculation of the volume fractions V_k, V_{buf}, and V_{ILTI} using Eqs. 5-3, 5-4, and 5-5, respectively:

$$V_k = [R_k/(R_k + R_{buf} + R_{ILTI})]^3 \quad , \tag{5-3}$$

$$V_{buf} = [(R_k + R_{buf})/(R_k + R_{buf} + R_{ILTI})]^3 - V_k \quad , \tag{5-4}$$

$$V_{ILTI} = 1 - V_k - V_{buf} \quad , \tag{5-5}$$

where R_k = kernel radius = 1/2 kernel diameter (μm),
R_{buf} = buffer thickness (μm),
R_{ILTI} = ILTI thickness (μm).

3. Calculation of the bulk density (D_b) of the ILTI coating using Eq. 5-6:

$$D_b = D_{sf}\left\{1 - \frac{(P)\ (0.00116)\ [D_k V_k + D_c\ (1 - V_k)]}{V_{buf}}\right\} \quad , \qquad (5\text{-}6)$$

where P = porosity as measured by Hg intrusion in units of μℓ/g of particles,
D_{sf} = sink-float density of ILTI.

4. Calculation of the buffer bulk density (D_{buf}) using Eq. 5-7:

$$D_{buf} = \frac{D_c(V_{buf} + V_{ILTI}) - D_b V_{ILTI}}{V_{buf}} \quad . \qquad (5\text{-}7)$$

From these data, the buffer void volume P^* in units of μℓ/g of kernel weight can be calculated from Eq. 5-8:

$$P^* = (1/D_{buf} - 1/2.2)\left(\frac{D_{buf} V_{buf}}{D_k V_k}\right)(1000) \quad , \qquad (5\text{-}8)$$

where 2.2 equals the theoretical density of carbon assumed for the ultimate density of the buffer carbon.

The necessary input measurements for these equations are obtained by QC measurements as given in the operating procedure. The calculations can be performed on the Univac 1110 computer using the program entitled VOID-VOLUME.

The buffer void volumes for two batches of ThO_2 fuel particles (6157-08-29T and 6157-08-37T) were measured. The data for these samples as measured using standard QC techniques are given in Table 5-4. The buffer void volumes for these samples were calculated and are given in Table 5-5. The two sets of results in Table 5-5 (1.55 and 2.2 g/cm^3) refer to the assumed ultimate density of the carbon in the buffer. As it is uncertain what the ultimate density of this carbon is, both the lowest density (as determined by mercury porosimetry) and the highest density (theoretical) results are presented.

The buffer void volume data were compared to measurements made on BISO coated 500-μm ThO_2 (Ref. 5-10). These data are shown in Table 5-6 assuming a buffer carbon density of 1.55 g/cm^3. Similar results have been calculated assuming that the ultimate carbon density is 2.2 g/cm^3. In Figs. 5-6a and 5-6b, the percent buffer void volume loss after ILTI coating versus buffer thickness is plotted for both sets of results. As can be seen from the least-squares fit lines in these two figures, the thicker the buffer coating, the less the percentage void volume loss. Thus, thin buffer coatings can lose as much as 50% of their void volume during ILTI coating, while very thick coatings may lose only about 10%. It can also be noted that the correlation coefficients shown in the two figures ($\sim$75%) are good correlations, considering the many measurements performed to obtain the void volume calculational data. If improvements could be made in the measurement of kernel diameter, buffer thickness, OLTI porosity, etc., the data scatter could probably be reduced.

These data demonstrated that the loss in buffer void volume is proportional to the thickness of the buffer layers. The data also showed that the buffer void volume after deposition of the ILTI coating can be measured for MEU and other types of fuels. It is important that the loss in buffer void volume be considered in the design of the buffer coating thickness for MEU fuels for FSV.

TABLE 5-4
DATA FOR SAMPLES OF ThO_2 FUEL

Batch No.	Kernel Diameter (μm)	Buffer Thickness (μm)	Buffer Density (g/cm^3)	ILTI Thickness (μm)
6157-08-29T	352	115	0.998	34
6157-08-37T	357	118	1.061	41

TABLE 5-5
BUFFER VOID VOLUME OF ThO_2 FUEL SAMPLES

Batch No.	Buffer Void Volume (μℓ/g ThO_2)	
	1.55 g/cm^3	2.2 g/cm^3
6157-08-29T	97.8	171.5
6157-08-37T	105.9	181.5

TABLE 5-6
COMPARISON OF BUFFER VOID VOLUMES

Batch No.	Kernel Diameter (μm)	Buffer Thickness (μm)	Void Volume at 1.55 g/cm^3 Carbon Density (μℓ/g ThO_2)		Void Decrease After ILTI Coating (%)
			Before ILTI	After ILTI	
6157-08-29T	352.3	115.0	123.6	97.8	21
6157-08-37T	356.8	118.2	114.1	105.9	7
6542-09-015	519.5	89.17	45.7	27.1	41
6542-16-015	501.2	38.58	16.7	11.4	32
6542-17-015	507.5	44.97	24.7	12.8	48
6542-18-015	499.6	87.77	41.4	37.7	9
6542-27-015	505.3	87.00	42.3	32.2	24
7366-117 "thin"	519.0	35.4	14.6	6.7	54
7366-117 "thick"	525.6	78.6	34.1	22.8	33

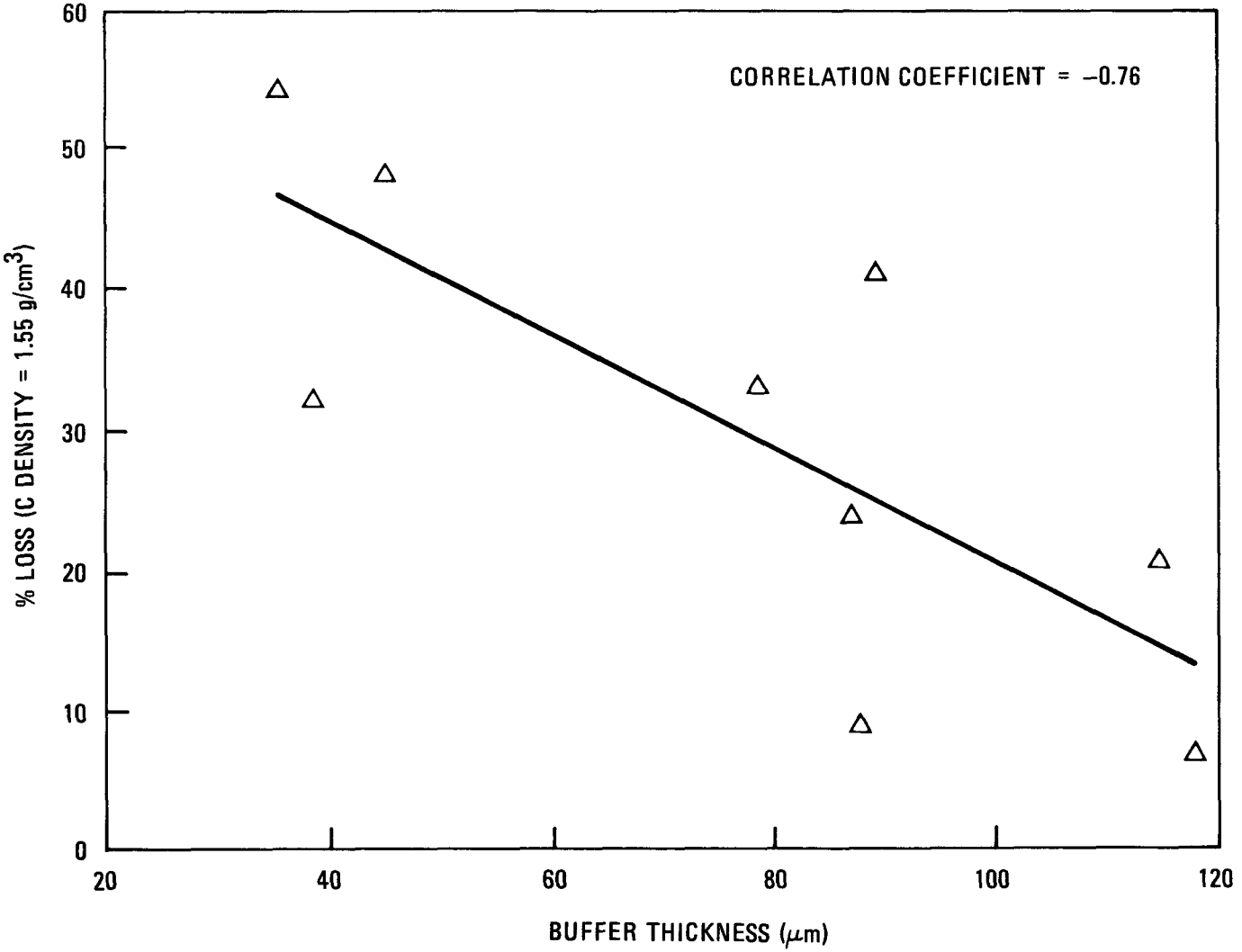

Fig. 5-6. Buffer void volume loss: (a) C density = 1.55 g/cm^3

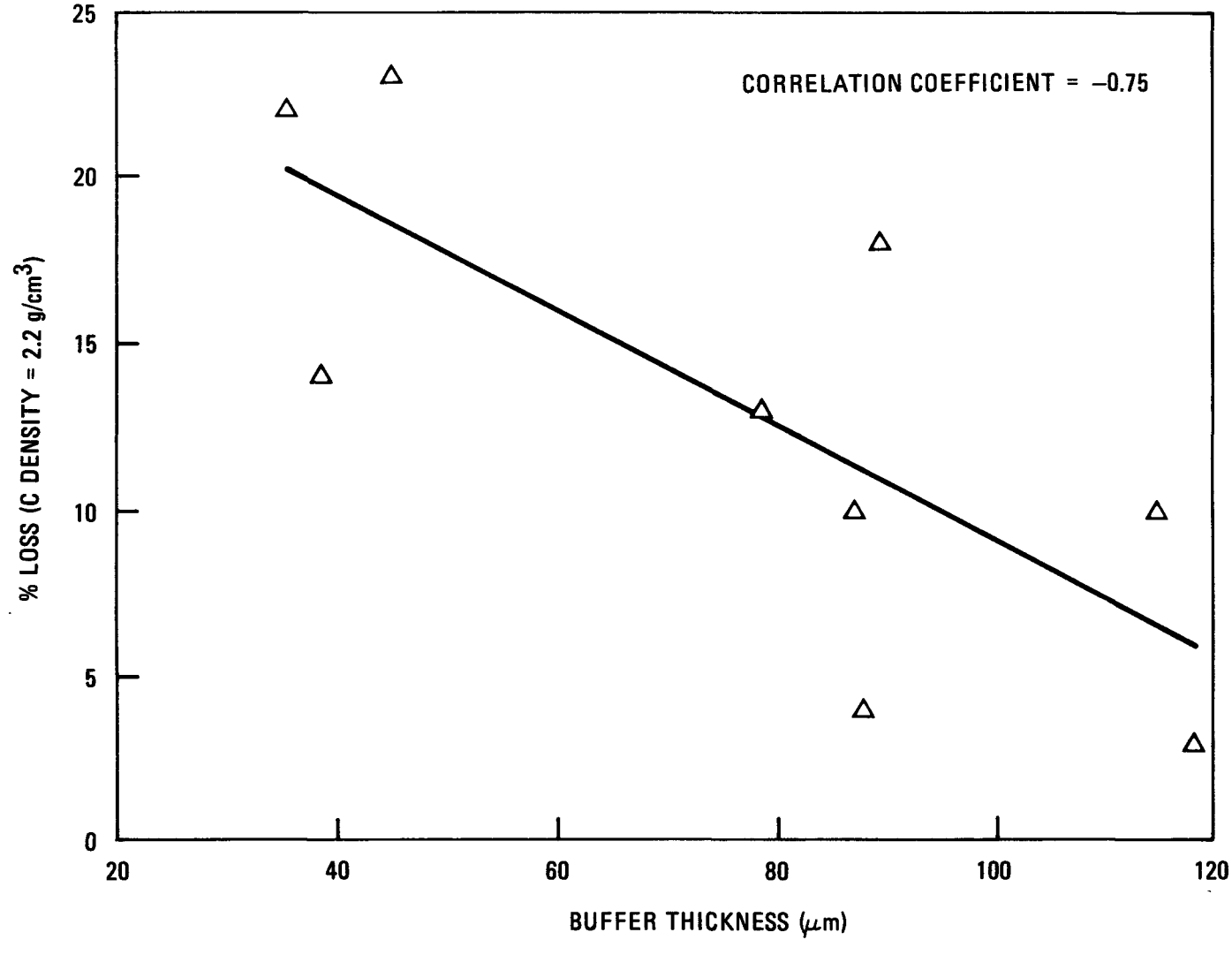

Fig. 5-6. Buffer void volume loss: (b) C density = 2.2 g/cm^3

5.4.3. QC Measurement Technique for SiC Coating Strength and Flaws

It has been of considerable concern that the numerous void areas (gold spots) in the SiC coating result in a substantial reduction in the SiC rupture strength. An effort was made to devise a QC method to measure the number of gold spots in the SiC coatings and the rupture strength of the SiC coatings. The review of all potential QC techniques led to the conclusion that a routine QC method to measure these attributes would be very difficult. The FMB has investigated a technique to measure half-shell SiC tensile rupture strengths with a high-pressure hydraulic system (Ref. 5-1). The SiC shells were pressurized with oil until they ruptured. The result of this work led to the following conclusions:

1. The tupture strength of SiC coatings appears to be influenced primarily by the degree of particle faceting. SiC coating flaws and SiC density do not significantly affect the SiC coating strength, as originally speculated. [This statement is obviously not true if the materials have very large SiC coating flaws and/or below specification SiC coating density ($\leq$3.18 g/cm^3)].

2. The primary item for additional QC method development in the SiC coating strength area is to increase the sensitivity of the faceting (aspect ratio) technique for measuring nonspherical particles. Doublet particles are extremely susceptible to SiC coating failure. Removal of doublet particles by liquid fractionation or process development is essential to assume good SiC coating behavior during irradiation.

The need to develop a routine QC technique to measure the rupture strength of the SiC layer has been eliminated. The simple compression point load breakage QC test or the tensile strength rupture method used by the FMB can be used for fuel process development on MEU fuel particles if further definition of the problem is required. It is recommended that

the faceting test (aspect ratio QC test) be used to control TRISO coated particle shape to assure good control of the SiC coating strength for MEU fuels.

5.4.4. Residual Chloride in TRISO Coated Particles

The presence of residual chloride in TRISO coated fuel particles after deposition of the SiC coatings has been attributed to premature SiC coating failure during irradiation (Ref. 5-2). The failure mechanisms have been speculated to be of the following types:

1. Transport of heavy metal chlorides to the SiC coatings with attack of the SiC by fission products and recoil fission fragments.

2. Transport of rare earth fission products (palladium) to the SiC inner surfaces with sequential attack.

3. Direct attack of the SiC layers by the reaction with free chloride ions.

The source of the chloride is speculated to be the diffusion of HCl during the initial SiC deposition on buffer/ILTI substrate with gas-permeable ILTI layers.

Several batches of TRISO coated UC_2 fuel particles which showed high and low SiC coating failures in the P13R and P13S capsules were selected for analysis for residual chloride. Pyrohydrolysis residual chloride and scanning electron X-ray emission analyses were conducted on these samples. The pyrohydrolysis data for these samples are given in Table 5-7. Particle mounts and fracture coated fuel particles from selected particles from these batches were also submitted for scanning electron X-ray emission

TABLE 5-7
PYROHYDROLYSIS ANALYSIS OF P13R AND P13S PARTICLES

Irradiation Sample No.	SiC Failure	Cl (ppm)
6151-17-025		
Aliquot No. 1	Low	<12
No. 2	Low	<23
No. 3	Low	<22
No. 4	Low	<26
6151-12-015		
Aliquot No. 1	Low	<13
No. 2	Low	<27
No. 3	Low	<26
No. 4	Low	<16
No. 5	Low	<20
No. 6	Low	<26
No. 7	Low	<19
No. 8	Low	<32
No. 9	Low	<26
6151-00-035		
Aliquot No. 1	High	<11
No. 2	High	<25
No. 3	High	<19
No. 4	High	<19
6151-02-025		
Aliquot No. 1	High	<15
No. 2	High	<19
No. 3	High	<22
No. 4	High	<26
6151-00-010		
Aliquot No. 1	High	<17
No. 2	High	<31
No. 3	High	<21
No. 4	High	<19
No. 5	High	<19
No. 6	High	<17
No. 7	High	<21
No. 8	High	<12
No. 9	High	<20
No. 10	High	<26

analyses. No chloride was detected in any of these samples. The data from both types of analysis showed the following:

1. The levels of residual chloride in these UC_2 TRISO coated batch samples were in the range of $\leq$30 ppm.

2. No differences in residual chloride levels were noted between samples with high and low SiC coating failure during irradiation.

On the basis of these data, the presence of high levels of residual chloride in the TRISO coated fuel particles could not be attributed to the levels of SiC coating failure. Better definition of this problem is needed before any additional QC method work is warranted. No recommendations can be made for MEU fuels until this problem is understood. The pyrohydrolysis QC technique appears to be the most economical method for this measurement. If residual chloride analysis of MEU fuels is required, then additional evaluation of this technique is recommended.

5.5. REFERENCES

5-1. "HTGR Fuel Development Department, Technical Status Report for the Quarter Ending December 1978," General Atomic unpublished data, March 30, 1979.

5-2. Homan, F. J., et al., "Irradiation Performance of HTGR Fuel Rods in HFIR Experiments HCB-9 and 10," DOE Report ORNL-5254, Oak Ridge National Laboratory, April 1978.

5-3. Whiting, C. D., "Preliminary Report on Techniques for the Determination of Residual Chlorides within Coated Fuel Particles," General Atomic unpublished data, September 18, 1978.

5-4. Mosen, A. W., et al., "Determination of Chlorine in Hydrogen Chloride Treated Fuel Rods," Gulf General Atomic unpublished data, December 21, 1971.

5-5. Adams, C. C., "The Potential Use of the Fluidized Particle Bed Washer/Dryer Apparatus as a Fractionating Unit to Produce Fuel Particles with Low Levels of Defective Coatings for Manufacturing Clean Fuels," General Atomic unpublished data, June 6, 1977.

5-6. Adams, C. C., "Demonstration of the Liquid Fluidized Particle Bed Fractionation System to Remove Defective Particles from TRISO Coated Fertile B ThC_2," General Atomic unpublished data, April 11, 1978.

5-7. Adams, C. C., "Further Data Analyses of the Particle Fractionation Study Conducted with the Fluidized Bed System," General Atomic unpublished data, May 8, 1978.

5-8. Boden, R. J., "Liquid Fluidized Particle Bed Fractionation System Demonstration with TRISO Coated MEU-type ThO_2 Particles," General Atomic unpublished data, October 24, 1978.

5-9. "Buffer Void Volume - MEU Fuels," General Atomic unpublished data, October 9, 1978.

5-10. Boden, R. J., "Buffer Porosity and Related Properties as Related to Buffer Thickness," General Atomic unpublished data, May 12, 1977.

6. FISSION GAS RELEASE FROM MEU FUEL KERNELS AND LASER-FAILED MEU TRISO PARTICLES

In support of the MEU fuel development program, measurements have been made of the R/B values for Kr-85m at 1100°C from various MEU (19.5% enrichment) fuel kernels and laser-failed MEU TRISO particles which were prepared for irradiation testing in FSV test elements 2, 4, and 6 and in capsules HRB-14 and HRB-15B (ORNL HFIR reactor). The R/B values obtained are summarized in Table 6-1.

TABLE 6-1
R/B VALUES FOR MEU FUEL KERNELS AND LASER-FAILED MEU TRISO PARTICLES

Fuel Composition	Kernel Diameter (μm)	Kernel Density (g/cm^3)	R/B, Kr-85m, 1100°C (%)	
			Kernel	Laser-Failed TRISO Particle
ThO_2-UO_2	357	10.40	5.3	0.05
UO_2	311	10.78	4.2	0.08
Uranium oxycarbide				
$UC_{0.71}O_{0.54}$	324	11.91	4.4	0.45
$UC_{0.50}O_{1.09}$	341	10.65	4.6	0.35
$UC_{0.28}O_{1.66}$	368	10.54	2.0	0.17
UC_2	345	11.04	6.1	1.66

Of the three types of uranium oxycarbide kernels studied, both the $UC_{0.71}O_{0.54}$ and the $UC_{0.50}O_{1.09}$ kernels consist of a mixture of UO_2 phase and an oxygen-containing uranium monocarbide phase. During the TRISO coating process, however, the monocarbide phase was converted to UC_2 by reaction with the porous carbon buffer. The $UC_{0.28}O_{1.66}$ kernels contain a mixture of UO_2 phase and UC_2 phase; therefore, no reaction with the porous carbon buffer occurred during the TRISO coating process.

The difference in the R/B values of the various MEU kernels studied does not appear to be significant. For the laser-failed TRISO particles studied, however, the R/B values increase in the order of oxide kernels < oxycarbide kernels < carbide kernels. This difference could be due to the higher susceptibility to hydrolysis of the UC_2 phase, which may have occurred to a certain extent after laser-failing and prior to R/B measurements.